Gas stripping in galaxy clusters: a new SPH simulation approach

P. Jáchym[1], J. Palouš[1], J. Köppen[1,2,3,4], and F. Combes[5]

[1] Astronomical Institute, Academy of Sciences of the Czech Republic, Boční II 1401, 141 31 Prague 4, Czech Republic
email: jachym@ig.cas.cz, palous@ig.cas.cz
[2] Observatoire Astronomique de Strasbourg, 11 Rue de l'Université, F–67000 Strasbourg, France
email: koppen@astro.u-strasbg.fr
[3] International Space University, Parc d'Innovation, 1 Rue Jean-Dominique Cassini, F–67400 Illkirch-Graffenstaden, France
[4] Institut für Theoretische Physik und Astrophysik, Universität Kiel, D–24098 Kiel, Germany
[5] Observatoire de Paris, LERMA, 61 Av. de l'Observatoire, 75014, Paris, France

Abstract. We present the results of numerical simulations of gas stripping in clusters, using N-body and SPH techniques adapted for two different gas phases, the diffuse and hot ICM and the denser and colder ISM. We compare the stripping efficiency with analytical approximations and with Gunn & Gott (1972) formula. Early and late type galaxies in large or small galaxy clusters show different stripping efficiencies, reaccretions and final masses dependent on the duration of the interaction. We discuss the origin of ICM and its large metallicity.

Key words. Galaxies: general – Galaxies: interactions — Galaxies: intergalactic medium — Galaxies: clusters: general

1. Introduction

Galaxies in clusters and rich environments are observed to be stripped of their interstellar medium (ISM), which quenches subsequent star formation. The stripping can be due either to tidal interactions, spiral galaxy mergers into ellipticals, or ram-pressure stripping from the intracluster gas (ICM). Both tidal and ram-pressure stripping are always tightly linked. Gunn & Gott (1972) assume that after the formation of a galaxy cluster, the remaining gaseous debris are thermalized via shock heating to virial temperatures corresponding to random motions in the cluster, e.g. to a few times 10^7K. This hot plasma at densities of a few times 10^{-3} cm^{-3} influences the ISM in disks of spiral galaxies, and can remove part of their gas through the ram pressure induced by the galaxy motions through the ICM.

The ram pressure stripping is difficult to model, since several complex gaseous phenomena are involved. The first aspect is the simple pressure force, and this can be modelled with a simple algorithm, with ballistic and sticky particles, to represent the gas (e.g. Vollmer et al. 2001). But the full hydrodynamical processes include thermal evaporation, turbulent and viscous stripping, and also outflows due to star formation.

The first note on the three-dimensional N-body/SPH simulations with the gravity tree to mimic the dynamical effect of the ram pressure on galaxies in clusters is by Kundić et al. (1993). The same approach has been adopted by Abadi et al. (1999). The ICM is represented as a flow of particles along a cylinder of radius 30 kpc and thickness 10 kpc. A spiral galaxy is in face-on, edge-on or an inclined orientation relative to flow of ICM particles. They examine with the simulations the radius up to which the ISM is removed and compare the results with the prediction of Gunn & Gott (1972) that the ISM is removed from the disk if the ICM ram pressure exceeds the restoring force:

$$\rho_{\rm ICM} v^2 \geq \left.\frac{\partial \Phi(r,z)}{\partial z}\right|_{\rm max} \Sigma_{\rm ISM}, \qquad (1)$$

where $\rho_{\rm ICM}$ is the ICM density, v is the relative velocity of the galaxy and the ICM, $\Phi(r,z)$ is the total gravitational potential of the galaxy as a function of the galactocentric cylindrical coordinates, and $\Sigma_{\rm ISM}$ is the ISM surface density. The conclusion is that Eqn. 1 applies in the face-on galaxy orientation when the bulge does not dominate over the disk gravity. In other cases, edge-on orientation and in central parts of galaxies, where bulge dominates, the stripping is less efficient. The time-scale for gas removal is $\sim 10^8$ years.

The ISM is far from continuous: it consists of several components: hot, warm and cold medium. Hot ionized and

warm neutral HI medium are much more continuous compared to cloudy, cold and molecular component. The SPH description relates more to the continuous ISM components, molecular clouds are not represented well in the SPH simulations. Vollmer et al. (2001) adopted another approach: they use N-body simulations with sticky particles representing the inelastic collisions between molecular clouds. The ram pressure is included with an additional friction force acting on clouds in the wind direction. Vollmer et al. (2006) introduced a time dependent ram pressure, which corresponds to the variations of the ICM density and of relative ICM - ISM velocity along the galaxy orbit in the cluster. They allow a moving ICM, which may increase its velocity relative the ISM to values higher than 4000 km s^{-1}.

With an isothermal SPH gas model, Abadi et al. (1999) show that gas stripping can be quite efficient in the core of rich clusters, on a time-scale of 10^7 yrs. The most efficient is face-on orientation. With an Eulerian code, Quilis et al. (2000) probed the efficiency of viscous coupling, enhanced by the presence of HI deficiencies in the center of galaxies. The ram pressure stripping does not depend strongly on the vertical structure and thickness of the gas disk (Roediger & Hensler 2005). In more details, the effect of inclination of the moving galaxy is important as long as the ram pressure is comparable to the gas pressure in the galaxy plane. In general the effect is similar for all inclinations except for edge-on (Roediger and Brüggen 2006). The orientation of the gas tail behind the galaxy is not a good tracer of the galaxy motion on its orbit. Acreman et al (2003) simulate the infall of an elliptical galaxy, and its gas stripping by the ICM: the formation of an X-ray wake at the first passage should be observable.

The principal competing mechanism to perturb galaxies in clusters and strip their gas is tidal interactions. High speed galaxy encounters in clusters, galaxy harassment events are efficient mechanisms to disturb galaxy disks, and provide stars to the intracluster space (Moore et al. 1995). Also low speed galaxy encounters in groups before the formation of the cluster are able to drag out tidal stellar tails and lead to galaxy mergers and formation of ellipticals, that are then known to be more numerous in clusters. The evolution of encounter debris in galaxy haloes has been followed by Mihos (2004).

Intracluster light is a consequence of tidal stripping of galaxies. It has been determined that intra-cluster stars are older than galaxy stellar populations, and more centrally concentrated in the cluster. The fraction of stars in the ICM is increasing with the richness of the cluster, it is usually a few percent of all stars, up to 20% (Arnaboldi et al. 2003, Murante et al. 2004). If the ICM metallicity can be explained partly by gas stripping from galaxies (Domainko et al. 2005), it can also come from intra-cluster supernovae exploding in the ICM. The irregular structures in galaxy clusters found in X-ray are tracing cold fronts and shocks due to galaxy interactions, or the infall of a group.

The fate of the stripped ISM in clusters is not clear: it can end very hot and become part of the ICM, or it can stay quite cold condensing into clouds with a molecular core and an HI outer boundary. Oosterloo and van Gorkom (2005) observe a large HI cloud near the center of the Virgo cluster, and suggest that this cloud has been ram-pressure stripped from the galaxy NGC 4388. The dense clumps in the HI plume might be molecular, and star formation could occur precisely at these high density places.
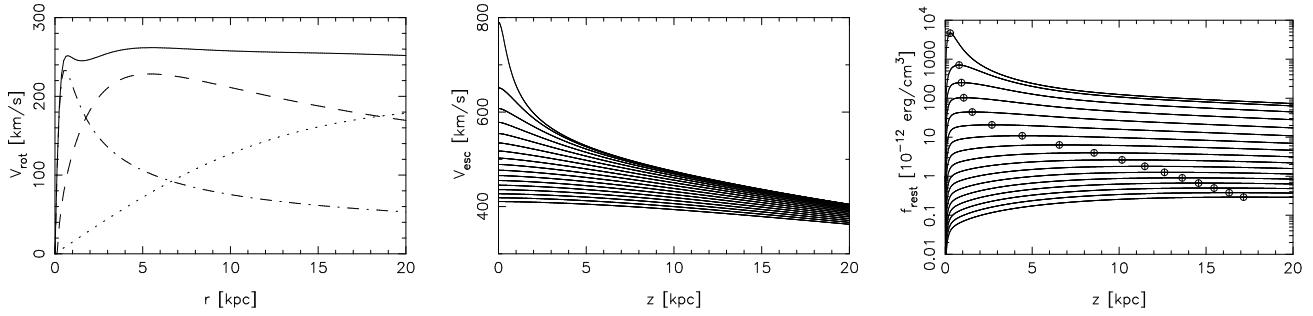
In this paper, we focus on computations of the ram pressure stripping, to evaluate more precisely its efficiency and to determine the fate of the stripped gas. The goal is in particular to take into account the finite time for this stripping interaction, as the galaxy passes quickly through the central region of the cluster. Most computations until now were carried out in the hypothesis of a stationary wind of hot gas. But the ram-pressure acts only in a short lapse of time, as simulated by Vollmer et al. (2001). After this short period, certain fraction of the gas falls back onto the galaxy. These latter simulations did not take into account the pressure forces, and the hydrodynamical physics of the ISM-ICM interactions. Roediger, Brüggen & Hoeft (2006) have followed the wake of gas produced by a quasi-stationary wind; in the present work, the impulsive character of ram pressure stripping is on the contrary emphasized.

Assuming a static ICM described with a β-profile, we explore in detail the ISM-ICM during the galaxy crossing the central part of the cluster. The mass-loss rates are examined as a function of the galaxy type, size and mass. We are able to follow the gas stripped from the galaxy, forming a giant tail of material. We tackle the issue of the origin of the ICM, the actual role of gas stripping in building it, as a function of the cluster mass and richness. The importance of gas stripping could account for the metal enrichment of the ICM as a function of cluster type (e.g. Domainko et al. 2005, Schindler et al. 2005). After presenting the model of stripped galaxies and of the cluster in sections 2 and 3, we introduce the initial conditions in section 4, and we describe our simulation method in section 5. In section 6, we discuss the results of the numerical simulations, the simulation test are shown in section 7, the equation of motion of an individual ISM gas element and the impulse approximation are given and applied to stripping in section 8. The present simulations are compared to other simulations in section 9. Section 10 presents the discussion and conclusion.

2. The galaxy model

Our model of a spiral galaxy is in a standard three-component halo + bulge + disk configuration. The halo and bulge components are given with spherically symmetric Plummer density distributions

$$\rho_{b,h}(r) = \rho_0 \frac{a_{b,h}^5}{(r^2 + a_{b,h}^2)^{5/2}}, \qquad (2)$$

Fig. 1. LM model galaxy. Left: Rotation curve with contributions of the halo (dotted), bulge (dash-dotted), and disk (dashed) components. Center: Escape velocity v_{esc} as a function of the z-distance behind the disk plane for 16 radii r starting with $r = 1$ kpc (top curve) and a spacing of 1 kpc. Right: Gravitational restoring force f_{rest} as a function of z for 16 values of r. Maxima in z for individual radii are denoted with circles.

			LM	Lm	EM	Em
disk:	M_d	$(10^{10}\ M_\odot)$	8.6	4	3.1	1.5
	a_d	(kpc)	4	4	6	6
bulge:	M_b	$(10^{10}\ M_\odot)$	1.3	0.5	7.3	3.5
	a_b	(kpc)	0.5	0.1	1	1
halo:	M_h	$(10^{10}\ M_\odot)$	42	14	49	16.4
	a_h	(kpc)	20	20	25	25

Table 1. The disk, bulge and halo parameters for late (L) or early (E), massive (M) or low mass (m) type model of a spiral galaxy.

where $\rho_0 = 3M_{b,h}/4\pi a_{b,h}^3$ is the central density, r is the distance from the galactic center, M_b, M_h are total masses, and a_b, a_h are radial scaling factors corresponding to the bulge or halo.

The axially symmetric disk follows a Toomre-Kuzmin infinitely thin disk multiplied by a $\mathrm{sech}^2(z/z_0)$ term which defines its isothermal vertical profile

$$\rho_d(r,z) = \rho_0 \frac{a_d^3}{(r^2 + a_d^2)^{3/2}}\ \mathrm{sech}^2(z/z_0). \qquad (3)$$

where (r, z) are the galactocentric cylindrical coordinates, and a_d and z_0 are the disk scaling factors. The central density is determined by $\rho_0 = M_d/4\pi a_d^2 z_0$ with the total mass M_d of the disk.

We introduce model spiral galaxies of various types: late-type (L) or early-type (E), subdivided according to their total mass: massive (M) or low-mass (m). L-types have a very low bulge-to-disk mass ratios, compared to E-types, and M-types have a massive halo component compared to m-types. Thus we employ four models: LM, Lm, EM, and Em. The values of the model parameters are given in Table 1. The scale height of the disk is in all models $z_0 = 0.25$ kpc.

Our standard galaxy model is the LM-type. Its rotation curve, the escape velocity and the gravitational restoring force $f_{rest} = \Sigma_{\mathrm{ISM}} \times \partial \Phi(r,z)/\partial z$, where $\Phi(r,z)$ is the total gravitational potential including all components of the galaxy, i.e. the force attracting ISM elements towards the galaxy symmetry plane, are shown in Fig.1. The escape velocity is obtained as a function (r, z) from the potential: $v_{\mathrm{esc}}(r,z) = \sqrt{2|\Phi(r,z)|}$, it has always the maximum in the symmetry plane $z = 0$.
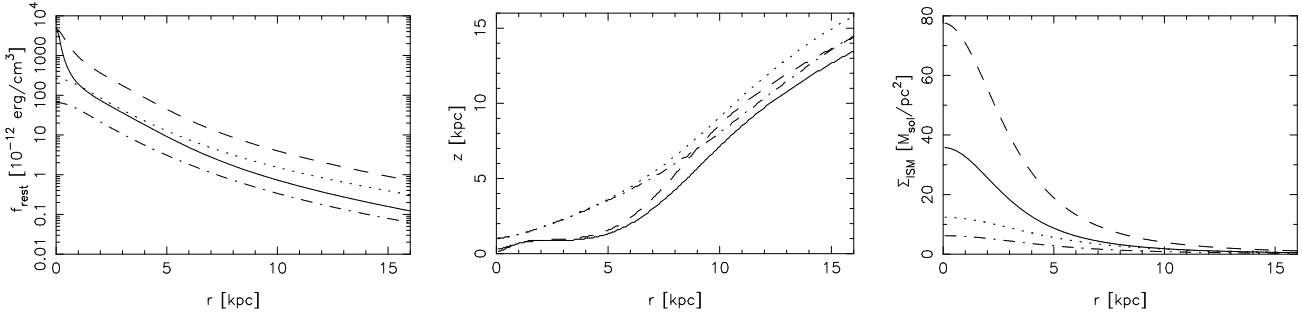
At a given r, the restoring force has a maximum at some distance z from the symmetry plane. This maximum is more and more distant from the $z = 0$ plane and its values decrease with the increasing radius r. In Fig. 2 (left panel) we plot the maxima of the restoring force as a function of r for different galaxy types. LM-type galaxy has a massive disk and massive halo which gives the highest restoring force compared to other galaxy types. Both, disk and halo are less massive in Lm-type, consequently the restoring force is smaller, only in the central part, where the very concentrated bulge dominates, the restoring force increases rapidly. The bulge is much more massive and extended in a EM-type galaxy, consequently the restoring force in the outer galaxy parts overcomes that of a Lm-type. For radii between 1 and 4 kpc, galaxy models Lm and EM show a very similar run of the maxima of the restoring force with r, but they are at lower z distances in Lm-type comparing to EM-type (see Fig. 2, central panel). The smallest restoring force has the Em-type galaxy, where disk and halo have lower masses compared to other types.

We assume that the ISM initially follows the density distribution of Eqn. 3 and that it amounts to 10% of the total disk mass. The ISM surface density Σ_{ISM} is plotted as a function of the galactocentric distance for the four galaxy types in the right hand panel of Fig. 2. The ISM is treated isothermally with $T_{\mathrm{ISM}} = 10^4$ K. A more detailed description of the initial conditions of simulations is given in section 4.

3. The model of a galaxy cluster

The hot ICM has been observed with X-ray satellites ROSAT and ASCA, and later it has been resolved spatially with satellites XMM Newton and Chandra (Böhringer 2004). The large scale ICM distribution in clusters is described with a β-profile (Cavaliere & Fusco-Femiano 1976; Schindler et al. 1999):

$$\rho_{\mathrm{ICM}} = \rho_{0,\mathrm{ICM}} \left(1 + \frac{R^2}{R_{\mathrm{c,ICM}}^2}\right)^{-\frac{3}{2}\beta_{\mathrm{ICM}}}, \qquad (4)$$
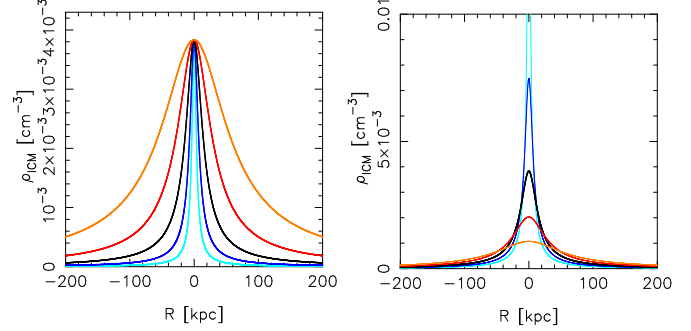
Fig. 2. Left: Maximum restoring force over z as a function of the galactocentric distance r for the four galaxy models adopted: LM (dashed), Lm (full), EM (dotted), and Em (dash-dotted). Center: Positions of the maximum values of the restoring force behind the disk plane for different radii r. Right: Surface density Σ_{ISM} of the ISM as a function of the galactocentric distance r.

where ρ_{ICM} denotes the ICM volume density at the distance R from the cluster center, $\rho_{0,ICM}$ is the volume density of the ICM in the cluster center, $R_{c,ICM}$ is a parameter of the ICM central concentration, and β_{ICM} is the slope parameter, which we set according to Schindler et al. (2001) to $1/2$.

The standard cluster has $\rho_{0,ICM} = 4\ 10^{-3}$ cm^{-3} and $R_{c,ICM} = 13.4$ kpc (cf. Vollmer et al. 1999). To model a rich galaxy cluster with a lot of hot ICM, or a poor cluster with just a little ICM in the center, we vary the values of $R_{c,ICM}$ and $\rho_{0,ICM}$. We multiply either standard value with factors of 0.25, 0.5, 1, 2, and 4. The total corresponding ICM mass within the inner 140 kpc (see later) of the cluster center then ranges between $2\ 10^9$ and $1.4\ 10^{11}$ M$_\odot$ (see Table 3).

The gravitational potential of a galaxy cluster is produced by the distributions of ICM and dark matter (DM) in the cluster. While ICM is described with the β-profile (Eqn. 4) with the above parameters, the DM is introduced through a similar β-profile. Having in mind the Virgo cluster, we set (cf. Vollmer et al. 2001), $R_{c,DM} = 320$ kpc, $\rho_{0,DM} = 1.6\ 10^{-2}$ cm^{-3}, and $\beta_{DM} = 1$ to correspond to the Virgo northern subclump about M87. The difference in the steepness of the gas and galaxy density profiles (β_{ICM} versus β_{DM}) corresponds well to observations, with the ICM density profile being steeper than the galaxy distribution in the inner part of the subclump. This implies $3.7\ 10^{12}$ M$_\odot$ or $1.4\ 10^{14}$ M$_\odot$ of DM within 140 kpc or 1 Mpc from the cluster center. Correspondingly, within the central 140 kpc, depending on the type of the cluster, the ICM represents from 0.05% to 30% of the mass. The ICM is treated adiabatically with initial temperature $T_{ICM} = 10^8$ K.

Fig. 3, left panel, illustrates the effect of the varying parameter $R_{c,ICM}$ for above mentioned five values 0.25, 0.5, 1, 2, 4 × 13.4 kpc. While the central density $\rho_{0,ICM}$ is fixed on the standard value, the width of the ICM density peak grows with increasing $R_{c,ICM}$. As a galaxy runs through the cluster it encounters a certain amount of the ICM. The right panel of Fig. 3 shows five clusters with such combinations of the parameters $R_{c,ICM}$ and $\rho_{0,ICM}$ that the galaxy moving on a completely radial orbit from 1 Mpc distance through the cluster center crosses the same
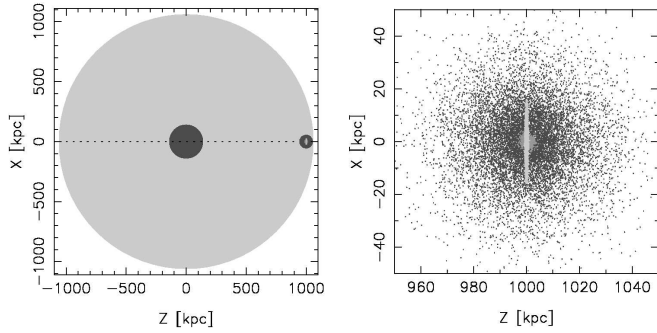

Fig. 3. Left: Central view of the ICM density distribution in clusters with $R_{c,ICM}$ equal to 0.25, 0.5, 1, 2, 4 × 13.4 kpc and $\rho_{0,ICM} = 4\ 10^{-3}$ cm^{-3}. Right: Peaks of the ICM density distribution with the following combinations of the β-profile parameters $(R_{c,ICM}, \rho_{0,ICM})$: (0.25, 3.82), (0.5, 1.95), (1, 1), (2, 0.53), and (4, 0.28) × (13.4 kpc, $4\ 10^{-3}$cm^{-3}). A galaxy traversing such clusters on a completely radial orbit from 1 Mpc distance crosses the same amount of the ICM.

amount of ICM. The shape of the peak changes from narrow and high to wide and low.

4. Initial conditions

The three components of the model galaxy are represented by a number of particles of equal mass: 12 000 for the halo, 6 000 for the bulge, and 12 000 for the stellar disk. Their initial distributions follow the density profiles of Eqns. 2 and 3. The components are cut off at 40 kpc, 4 kpc, and 16 kpc, in the case of the halo, bulge, and disk, respectively. The ISM is represented with 12 000 SPH particles of total mass equal to 10% of the total disk mass. This means that the mass of an ISM particle is in the range of $(1.5 - 5.7)$ 10^5 M$_\odot$ in the four introduced galaxy types. Their initial distribution follows the density profile of the stellar disk (Eqn. 3) (see right panel of Fig. 2).

The ICM of the cluster is modelled with 120 000 SPH particles following the β-profile (Eqn. 4) with a cut-off at $R = 140$ kpc from the center of the cluster (see below for explanation). The total mass of the ICM particles is derived from cluster parameters. With the parameters of the standard cluster, $\rho_{0,ICM} = 4\ 10^{-3}$ cm^{-3} and $R_{c,ICM} = 13.4$ kpc, there is $6\ 10^{10}$ M$_\odot$ of the ICM within

Fig. 4. Initial conditions of our simulations. Left: Starting position of a galaxy falling face-on to the cluster center (dashed trajectory). The ICM particles are distributed about the cluster center up to 140 kpc distance (dark). Outside this region the effect of the ICM is only gravitational (light). Right: Zoom on the initial configuration of the galaxy with the DM halo (black points), and the disk + bulge (grey shaded area).

N_{ICM}	$R_{c,ICM}$ (kpc)	$\rho_{0,ICM}$ (cm^{-3})	$T_{R=140\,kpc}$ Gyr	T_0 Gyr	v_0 (km/s)
120 000	13.4	$4\ 10^{-3}$	1.53	1.64	1260

Table 2. Standard simulation run. Values of the β-profile parameters of the ICM, times at which the galaxy enters the ICM, and reaches the cluster center, and its velocity in the cluster center are stated.

140 kpc from the cluster center, consequently the mass of an individual ICM particle is $\sim 5\ 10^5$ M$_\odot$, which is comparable to the mass of an ISM particle. For the LM–type galaxy and different clusters the mass ratio of ISM to ICM particles ranges between 30 and 0.04.

Fig. 4 shows the initial configuration of the system. The galaxy in face-on orientation relative to the orbit is located at the cluster periphery at 1 Mpc distance from the center, $\boldsymbol{R} = (x, y, z) = [0, 0, 1]$ Mpc, with no systematic velocity. Consequently, it freely falls towards the cluster center. Thus, in this paper, all the orbits are completely radial, free-fall orbits from the distance $R = 1$ Mpc to the cluster center. For the standard cluster, the galaxy reaches the cluster center after about 1.64 Gyr, at a velocity of about 1300 km s^{-1}. It means that it moves strongly supersonically through the ICM in the central regions. In our simulations, we follow the galaxy on its orbit during 2 Gyr. The galaxy enters the ICM distribution of the standard cluster at about 1.5 Gyr. Table 2 summarizes the parameters of the standard simulation run.

A more realistic simulation would spread the ICM particles throughout the cluster up to 1 Mpc radius so that the galaxy runs all its orbital time through the medium. However, as noted by Abadi el al. (1999), too massive ICM particles may become bullets punching holes into the ISM disk. To prevent this, the masses of individual ICM particles must at most be comparable to that of ISM particles. With this assumption and the number of ISM particles set to 12 000, the sphere of 1 Mpc radius of the cluster would need about 2 millions particles of the ICM. Consequently

the calculations would be very time-consuming, and the output data files huge.

To avoid this, we restrict the active sphere of the ICM distribution to central regions of the cluster, where the effect of the ICM-ISM interaction is strongest. We fill up the central cluster sphere to such a radius, at which the outskirts of the galaxy arriving from the cluster periphery starts to be affected by the steeply rising ram pressure of the ICM. According to our standard model, the cut-off radius is set to 140 kpc, outside which only the gravitational effect of the ICM to the galaxy is considered. From the very beginning at 1 Mpc distance, the galaxy itself evolves and thus instabilities and spiral arms form. Consequently, the galaxy enters the ICM sphere dynamically evolved.
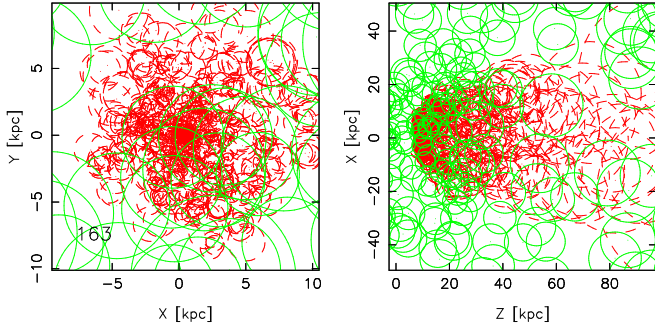
Along the radial orbit, we can compute the ram pressure $p_{ram}(R) = \rho_{ICM} v_{gal}^2$ acting on the galaxy as it moves through the ICM. The ram pressure always peaks in the cluster center where the density of the ICM is highest, and also where the orbital velocity has its maximum. Following Fig. 3, for broader clusters the increase of the ram pressure starts at larger distances from the cluster center. With the same central density $\rho_{0,ICM}$ the peak value of the ram pressure is slightly larger for broader clusters, which is caused by higher speed of the galaxy due to the contribution of the ICM to the overall cluster gravity (see Fig. 10, left panel).

5. Simulation method

We perform 3D tree/SPH N-body simulations using GADGET in version 1.1 (Springel et al. 2001). The tree method is a highly effective Lagrangian technique for computing gravity forces in non-homogeneous systems. The particles are arranged into groups hierarchically ordered from the smallest ones containing only one particle up to the biggest one embracing the whole system. The scheme of an oct-tree structure dividing the computational space into a sequence of cubes is used (Barnes & Hut 1986). Then, the gravitational force exerted by distant groups on a particle is approximated by their lowest multipole moments which reduces the computational costs to order $O(N \log N)$.

The Smoothed Particle Hydrodynamics (SPH, Lucy 1977, Gingold & Monaghan 1977) is a Lagrangian method for solving hydrodynamical problems in which real fluids are represented by a set of fluid elements, i.e. particles. The key idea of the SPH is that every particle has an effective radius within which hydrodynamical interactions with neighboring particles operates. Thus the particles are no longer point masses but are smoothed out and local hydrodynamical properties are interpolated from the local mass distribution. The smoothing sizes of particles are determined to correspond to a radius within which a given number of neighboring particles is contained.

GADGET in version 1.1 resolves only one gaseous phase and all gas particles occurring in the system are hydrodynamically treated as one group. However, the volume densities of the ISM in the disk and of the surround-

Fig. 5. SPH sizes of the ISM (dashed) and ICM (full) particles at the epoch when the galaxy runs through the cluster center. $N_{\mathrm{ICM}} = 120\,000$, $N_{\mathrm{ISM}} = 12\,000$. Left: Face-on zoom view of the galaxy surroundings with the ISM particles located within $\pm$ 2 kpc about the disk plane, and the ICM particles within $\pm$ 20 kpc about the disk plane. Right: Edge-on view of the situation with ICM particles located within $\pm$ 20 kpc about the disk in the line of sight direction. Only every tenth particle is displayed.

ing ICM differ by several orders of magnitude, as well as their temperatures. To treat correctly their interaction, the number densities of the ICM and ISM particles, n_{ICM} and n_{ISM}, should be comparable. Otherwise, the ICM particles located far from the galaxy would be larger in the SPH sense than the ISM particles, since the number of neighboring particles is kept constant throughout the system. When these large ICM particles would later approach the disk, their sizes would be re-evaluated from the local mixing of ICM and ISM particles, and artificial punching effects could follow.

To achieve a similar number densities of both gases, a huge number of ICM particles is necessary. Having in mind these constraints, we introduce a set of changes into GADGET related to the fact that we need to simulate two different gaseous phases (ICM, and ISM) with different spatial resolution. Firstly, the subroutine for searching the neighboring particles is adapted to distinguish between the two phases: the smoothing radii h's of either ICM or ISM particles are calculated separately from the neighbors of a corresponding phase. Since both phases are now treated separately, we can use a reasonable number of ICM particles. These particles are then substantially larger than the ISM and their size does not change even when interacting with the disk. It ensures that all the disk area is covered by the ICM particles. Secondly, the hydrodynamical interaction of the two phases can proceed. While in the previous step of evaluating the particle sizes, the ICM and ISM phases are searched separately in the sense that all neighboring particles of the second phase are omitted, and the search continues until N_b proper neighbors is found, now both phases are searched together to find all particles with $|\boldsymbol{r}_{ij}| < \max(h_i, h_j)$. A given ISM particle then interacts with all the ICM particles within which smoothing radii it is contained. Further, the adiabatical, and isothermal treatment of the ICM, and ISM is implemented, respectively.

Fig. 5 compares the ISM (dashed circles) versus ICM (solid circles) particle sizes in the surroundings of the galaxy running through the center of the standard cluster. $N_{\mathrm{ICM}} = 120\,000$ and $N_{\mathrm{ISM}} = 12\,000$, face-on and edge-on snapshots are displayed. Only every tenth particle is plotted, which gives the impression of voids occurring among particles. One notes that the size of the ICM particles is kept constant in the disk vicinity.
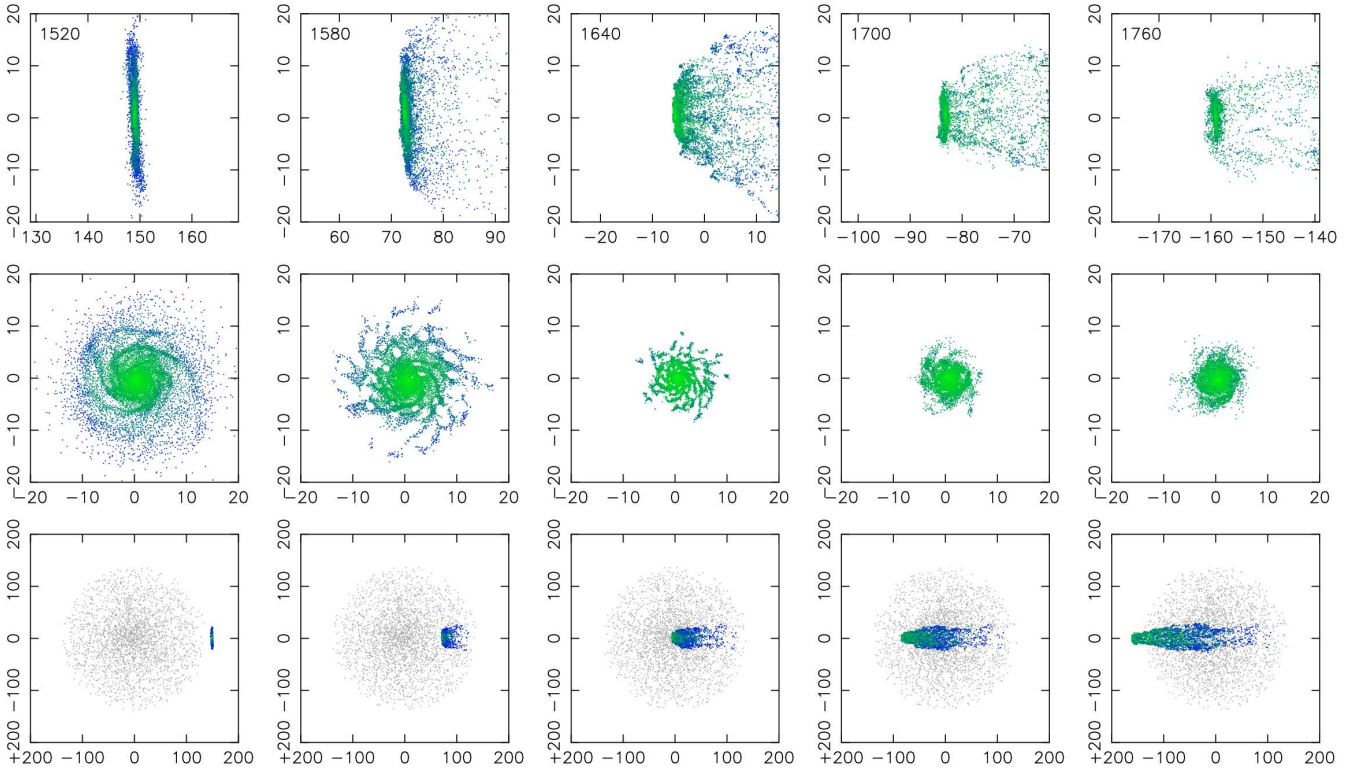
To achieve a sufficient spatial resolution in the disk, we fix the number of ISM particles N_{ISM} to an adequate value. In all simulations, the resolution in the disk is then the same. From Fig. 5 it follows that the ICM particles are substantially larger than their ISM counterparts, each of them covering a large part of the disk. That means that a group of close ISM particles lying within the smoothing radius of a given ICM particle feel only the ram pressure of the ICM but no pressure gradients, as it would be the case if the sizes of ICM and ISM particles were comparable. Then, in fact no detailed hydrodynamical effects are involved in the ISM-ICM interaction. However, in Sec. 7, Fig. 17, we discuss test runs with varying number of ICM particles, where these hydrodynamical interactions could occur. These tests show that the stripping results are practically independent of the N_{ICM} value.

This suggests that a detailed hydrodynamical treatment of the interaction is not so important at this stage, and only the ram pressure plays a crucial role in the stripping. Our simulation approach using only a reasonable number of ICM particles, and thus neglecting the detailed hydrodynamics in the ISM-ICM interaction treatment, has some similarities with the method of Vollmer et al. (2001), who in their sticky-particle simulations include the effect of the ram pressure only analytically as an additional acceleration on the ISM clouds located at the surface of the gas distribution. In our case, of course, the interaction between ICM and ISM is not restricted to the surface layer.

Our approach is more realistic than Vollmer et al. (2001) as far as the ICM is concerned. The ICM phase is treated fully hydrodynamically. Therefore, as will be discussed later, simulations develop a bow shock that forms in the ICM in front of the galaxy. Consequently, the incoming ICM particles are deflected from their direction to flow around the disk. Moreover, when (from the SPH point of view) small ISM particles are stripped out of the disk, their number density falls and their size increases. In the tail of stripped particles, the sizes of both the ISM and ICM become then comparable, and the hydrodynamical treatment of the tail is correct (see Fig. 5).

6. Simulation results

First we describe results of the standard simulation run (see Table 2) of the LM galaxy. This shows how the ISM of the galaxy changes under the influence of the evolving galactic gravitational field which includes the self-gravity of the ISM disk, the gravitational field of the cluster, which changes along the orbit, and under the influence of the
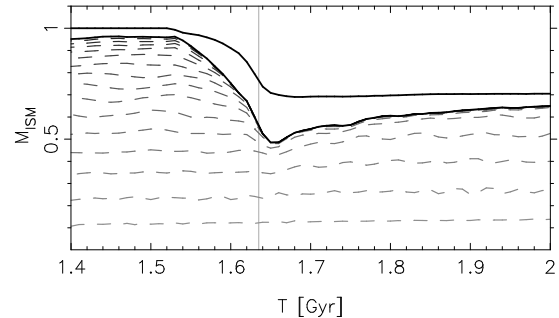
Fig. 6. Time sequence – a galaxy crossing the cluster center. The two upper rows show the edge-on and face-on views of the galaxy as it loses its outer parts, the lower row shows the motion through the center of the cluster filled with the ICM particles. The time since the beginning of the free fall from the cluster edge is given in Myr in the left upper corner of frames in the first row.

ram pressure due to relative motion of the ISM and ICM. We note that no effects of the ram pressure to the stellar disk, bulge or halo galaxy components are observed in the further simulations described below.

6.1. LM galaxy in the standard cluster

Fig. 6 displays snapshots of the ISM disk at five epochs of the galaxy's crossing through central parts of the cluster. Freely falling from the 1 Mpc distance, it approaches at time 1.52 the edge of the ICM particle distribution, where ram pressure rises. At 1.64 Gyr it passes through the cluster center and experiences the peak ram pressure. At 1.76 Gyr it leaves the ICM on the other side of its distribution, relaxes after the fade-out of the ram pressure, and further continues towards the second apocenter. Fig. 6 shows edge-on and face-on views of the ISM disk, and a wide view of the central parts of the cluster with the ICM particles.
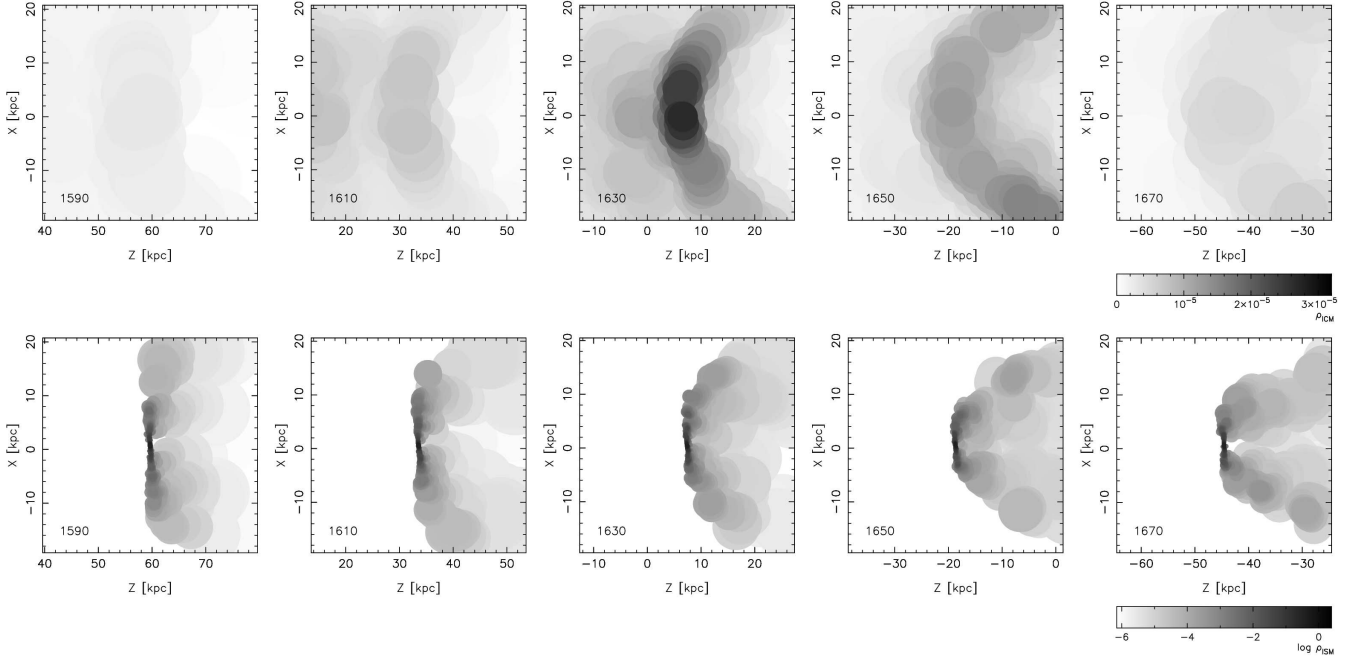
When the galaxy enters the ICM distribution, the local value of the ram pressure is sufficient to influence only the outer disk regions. The ISM from these regions is stripped and thus forms the end of the tail of stripped gas. Later on, also more inner parts get stripped by the increasing ram pressure, filling the central portion of the tail that is clearly visible in Fig. 6. The opening angle of the tail changes with time which reflects the time evolution of the ram pressure vs. restoring force contest. Schulz & Struck
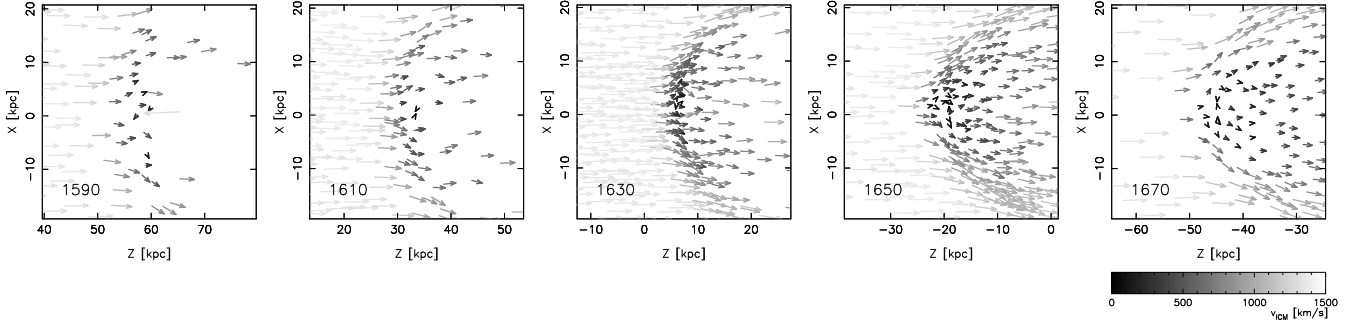

Fig. 7. The standard simulation run. Time evolution of the ISM mass within 16 different disk radii ($1 - 16$ kpc) and $|z| < 1$ kpc (dashed curves). The uppermost curve corresponds to the ISM mass bound to the galaxy. The instant of crossing the cluster center is marked with the vertical line.

(2001) describe an effect of the ram pressure enhancing the spiral structure of the disk since particles from inter-arm positions with lower surface densities are more easily removed. This effect is observed at time 1.58 Gyr.

The process of stripping is displayed in Fig. 7. It shows the number of ISM particles, i.e. the ISM mass, within different disk radii growing from 1 kpc to 16 kpc with a step of 1 kpc, and within a $|z| < 1$ kpc belt about the disk plane as a function of the orbital time. The uppermost curve shows the ISM mass M_{bnd} that is bound to the galaxy, i.e. the number of ISM particles with negative total energy. Before the galaxy enters the ICM zone

Fig. 8. Density of the ICM in surroundings of the LM-type galaxy (top) and of the ISM (bottom). A bow shock forms in front of the disk. Individual particles are displayed as filled circles with radii equal to their SPH smoothing sizes h's. The scale of the ISM density is logarithmic due to large differences in the disk plane and in the tail of stripped particles. The time in Myr is given in the left lower corner of frames.

Fig. 9. The flow of ICM particles around the LM-type galaxy. Vectors of relative velocity of ICM particles interacting with the ISM disk are displayed.
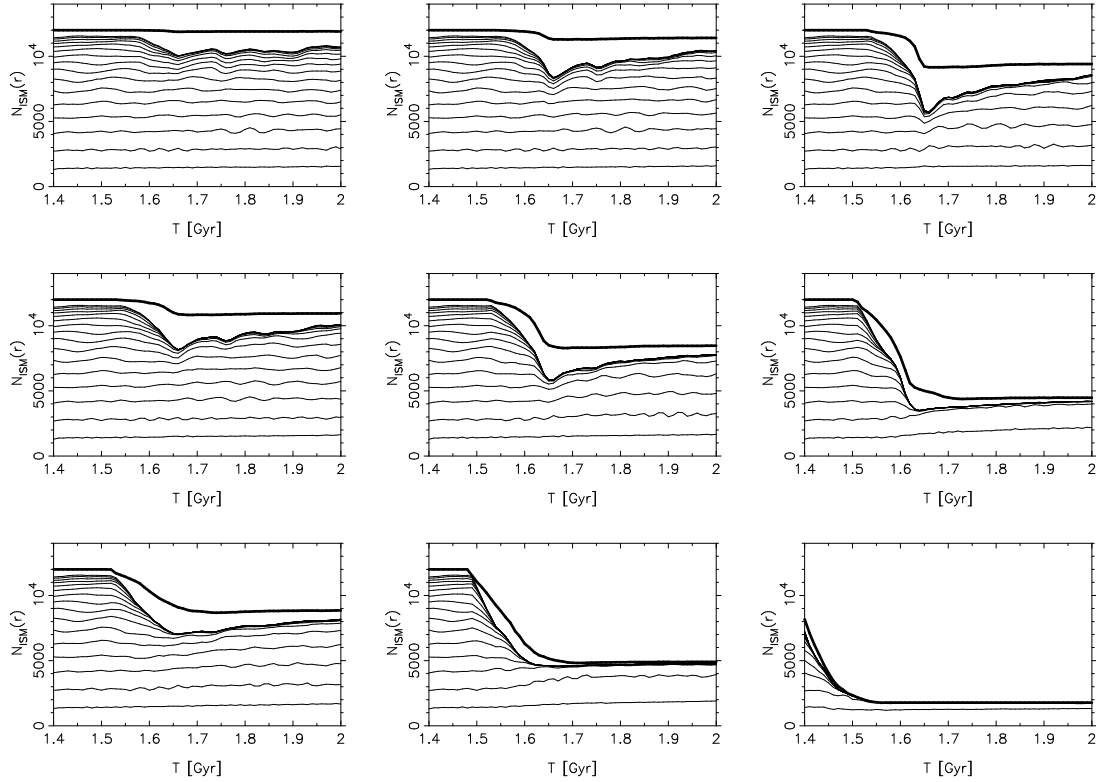
at ~ 1.53 Gyr, no important changes are observed. Once the ram pressure rises, particles from decreasing radii are shifted out of the evaluation belt. With a delay of about 20 Myr after the galaxy's passage through the center, a maximum amount of the ISM is shifted out of the $|z| < 1$ kpc zone, and curves in Fig. 7 show a minimum corresponding to 49% of the initial total ISM mass. Particles down to about 4 kpc are influenced. After the minimum, a strong reaccretion of the ISM occurs, concerning the ISM previously only shifted out of the disk by a short-term effect of the strongest ram pressure, but staying bound to the galaxy. Of course, both the minimum value and the amount of the reaccreted material depend on the definition of the evaluation zone.

With a constant flow of the ICM, Roediger & Hensler (2005) identify three phases of stripping: an instantaneous phase when the outer disk parts are bent in the wind direction but stay bound to the galaxy, a dynamic intermediate
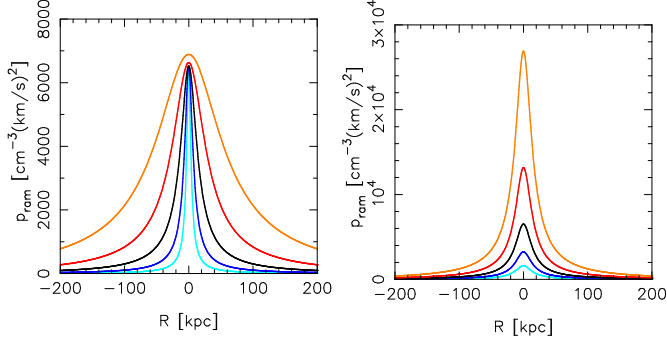
phase during which the bending breaks and a part of the ISM is stripped and another part falls back to the disk, and a quasi-stable continuous viscous stripping phase when the outer disk layers are peeled off by the Kelvin-Helmholz instability at a rate of ~ 1 M$_\odot$ yr^{-1}. The duration of the first phase is $\sim 20 - 200$ Myr, while the following second phase is about ten times longer. In our simulations, we observe a behaviour similar to the first two phases, however, the evolution of the $M_{\mathrm{bnd}}(t)$ and $M_{|z|<1\mathrm{kpc}}(t)$ under the operation of a peaked ram pressure is different (see Fig. 7). Once the ram pressure rises, the outer disk layers are released, while the more inner ones are only shifted from the $|z| < 1$ kpc zone. Although the rate of the release is lower compared to the shifting, both effect occur simultaneously. When the ram pressure ceases, the shifted but bound ISM reaccretes.

From Fig. 7 we determine the final post-stripping mass M_{final} of the galaxy as the mass of bound ISM at the

Fig. 11. Stripping of the LM–type galaxy crossing clusters with varying ICM distribution: from left to right: $\rho_{0,\mathrm{ICM}} = 0.25$, 1, 4 $\times$ 4 10^{-3} cm^{-3}, from top to bottom: $R_{\mathrm{c,ICM}} = 0.25$, 1, 4 $\times$ 13.4 kpc. See Fig. 7 for details. Simulations in the same row thus have a constant value of the $R_{\mathrm{c,ICM}}$ parameter and simulations in the same column keep the $\rho_{0,\mathrm{ICM}}$ value. Central panel corresponds to Fig. 7.

Fig. 10. Central views of the ram pressure peaks with a fixed $\rho_{0,\mathrm{ICM}} = 4\ 10^{-3}$ cm^{-3} and $R_{\mathrm{c,ICM}} = 0.25, 0.5, 1, 2, 4 \times 13.4$ kpc (left), and a fixed $R_{\mathrm{c,ICM}} = 13.4$ kpc and $\rho_{0,\mathrm{ICM}} = 0.25, 0.5, 1, 2, 4 \times 4\ 10^{-3}$ cm^{-3} (right).

final simulation time of 2 Gyr: $M_{\mathrm{final}} = 0.71 M_{\mathrm{d,ISM}}$. The stripping radius r_{strip} is more tricky to measure, since not all the reaccreting material is at the final simulation time back in the disk. We estimate it to $r_{strip} \sim 6$ kpc. Initially, in Fig. 7 about 5% of the 12 000 ISM particles is, due to relaxation processes and scattering on spiral arms, outside the region $r < 16$ kpc, $|z| < 1$ kpc already before the ram pressure starts to play a role. But all these particles have the negative total energy.

Fig. 8 shows in the upper row the ICM density distribution in the surroundings of the galaxy passing the densest parts of the cluster at times $1.59 - 1.67$ Gyr. The particles are displayed as filled circles with radii equal to their SPH smoothing lengths h's. The gray shade corresponds to the density. Due to the supersonic motion we see a bow shock forming in the ICM. It is most pronounced when the galaxy passes through the cluster very center. The bottom row of Fig. 8 shows the ISM density. Due to large differences in the density between the disk and the tail, the grey-scale is logarithmic. Note the growth of ISM particles when they are stripped from the disk. In Appendix, Fig. 21 shows the ICM and ISM density distribution in the case of simulation with $N_{\mathrm{ICM}} = 480\,000$.

Fig. 9 shows the velocity vectors of the ICM particles interacting with the ISM disk. At the surface of the disk, ICM decelerates from more than 1000 km s^{-1} to less than 100 km s^{-1}. We can also see the deflection of the ICM flow to the sides along the shock, and a low velocity ICM in the shadow behind the galaxy. Domainko et al. (2005) draw attention to the role of the bow shock: the ram pressure behind the shock is lower since there the relative velocities of the ICM particles are smaller than in front of the shock. On the contrary, Rasmussen et al. (2006) notice that while the ram pressure is reduced at the shock, $P_{th} + \rho v^2$, where P_{th} is the thermal ICM pressure behind the shock, stays conserved for an inviscid fluid, and thus the reduction of the ram pressure behind the shock is balanced by an increase in static thermal pressure. Therefore, the force per

$R_{c,ICM}$ (kpc)	$\rho_{0,ICM}$ (10^{-3}cm^{-3})	$M_{ICM}^{R<140\,\text{kpc}}$ $(10^{11}\,M_\odot)$	$\Sigma_{ICM}^{R<140\,\text{kpc}}$ $(M_\odot/\text{pc}^2)$	p_{ram}^{max} $(\text{cm}^{-3}\text{km}^2\text{s}^{-2})$	r_{strip} (kpc)	M_{strip} (%)	M_{min} (%)	M_{accr} (%)
	1	0.02	0.38	1 612	13.8	1	84	15
	2	0.04	0.76	3 231	12.8	2	78	20
3.4	4	0.08	1.53	6 453	11.8	5	70	25
	8	0.16	3.05	12 949	10.3	12	59	29
	16	0.32	**6.10**	25 900	7.5	22	48	30
	1	0.06	0.74	1 615	12.3	3	75	22
	2	0.11	1.47	3 233	11.2	7	68	25
6.7	4	0.22	2.94	6 480	8.7	14	57	29
	8	0.44	**5.87**	13 014	7.1	26	47	27
	16	0.89	11.76	26 229	4.5	41	36	23
	1	0.15	1.39	1 618	10.8	9	68	23
	2	0.30	2.78	3 245	8.4	16	59	25
13.4	4	0.61	**5.56**	6 524	6.3	29	49	22
	8	1.21	11.13	13 182	4.1	43	40	17
	16	2.43	22.26	26 894	2.6	63	29	8
	1	0.39	2.56	1 625	8.8	16	64	20
	2	0.78	**5.12**	3 272	7.0	27	55	18
26.8	4	1.57	10.25	6 631	5.0	44	44	12
	8	3.14	20.50	13 608	2.8	62	31	7
	16	6.28	40.99	28 604	2.5	80	20	0
	1	0.90	**4.52**	1 641	7.7	26	59	15
	2	1.80	9.04	3 336	5.0	42	47	11
53.6	4	3.61	18.08	6 888	3.5	59	38	3
	8	7.21	36.16	14 637	2.9	76	24	0
	16	14.42	72.29	32 722	2.4	85	15	0

Table 3. Summary of stripping results of the set of twenty-five simulations with the LM–type galaxy crossing clusters with varying values of the $R_{c,ICM}$ and $\rho_{0,ICM}$ parameters. Stripping radius r_{strip} of the ISM disk, mass of the stripped ISM M_{strip}, minimum mass of the ISM within the evaluation zone, and mass of the reaccreted ISM M_{accr} are stated. $M_{strip} + M_{min} + M_{accr} = 100\%$. Values of peak ram pressure p_{ram}^{max}, column density of the encountered ICM Σ_{ICM}, and mass of the ICM within central part of clusters M_{ICM} are added.

unit area acting on the disk is close to the pre-shock ram pressure. In Fig. 22 of the Appendix the ICM velocity field for the case of $N_{ICM} = 480\,000$ is shown.

6.2. LM galaxy in various clusters

As we have seen in Fig. 7, the stripping of the ISM is a dynamical process depending strongly on the shape of the ram pressure peak. Therefore, we present the results of a set of twenty-five simulations of the LM–type galaxy crossing clusters with varying distribution of the ICM.

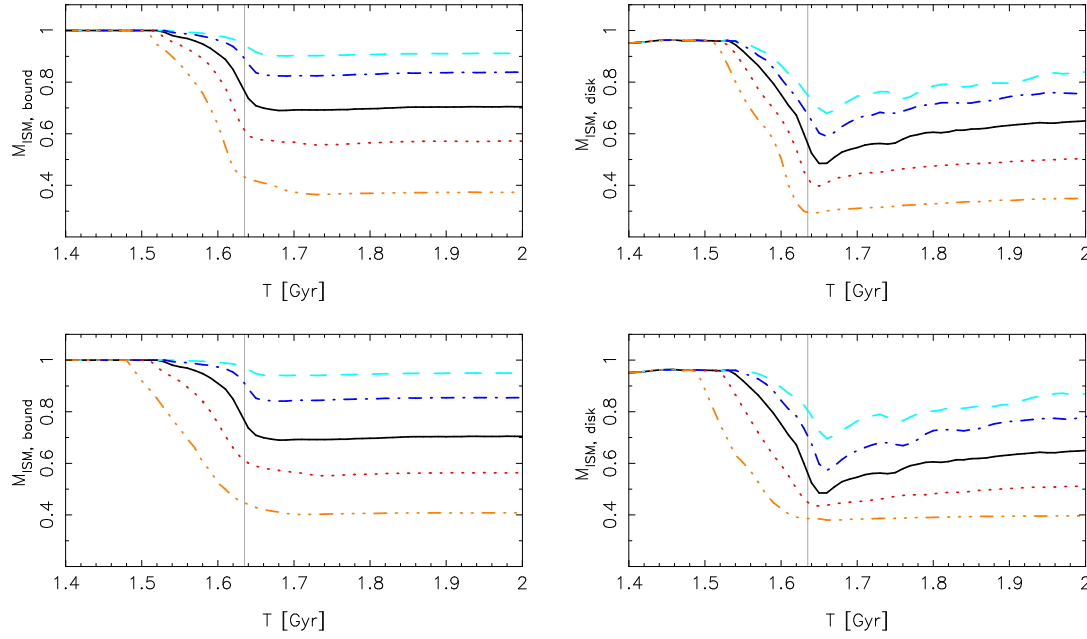### 6.2.1. Results from the simulations

Multiplying the standard values of the parameters $R_{c,ICM}$ and $\rho_{0,ICM}$ by factors of 0.25, 0.5, 1, 2, and 4, we study the effects of a varying width and height of the ICM density peak on the stripping results. Fig. 10 illustrates the ram pressure profiles corresponding to the ICM distribution with varying widths but a constant height (left), and varying heights but a constant width (right).

Fig. 11 shows the stripping results of nine runs from the above set of twenty-five simulations. Individual panels are of the type of Fig. 7 and correspond to $\rho_{0,ICM} = 0.25$,

1, 4 × 4 10^{-3} cm^{-3} (from left to right), and $R_{c,ICM} = 0.25, 1, 4 \times 13.4$ kpc (from top to bottom).

The main stripping event is in all the cases rather short and takes 100 to 200 Myr. Going from upper left corner to lower right corner of Fig. 11, the stripping expands to more and more inner parts of the galaxy. It means that both increasing width and height of the ICM density peak support the stripping. Nevertheless, the process of stripping itself is different in either direction:

a) Following a row, i.e. for a fixed value of the $R_{c,ICM}$, the minimum of the ISM mass deepens with growing value of the central density. In the upper row, the ram pressure peak is narrow, with $R_{c,ICM} = 3.4$ kpc. If the peak is not high (left), most of the ISM remains inside the $|z| < 1$ kpc layer. There is ∼ 12% of the ISM that has been shifted out of it, but almost all of it remains gravitationally bound to the galaxy and later will be reaccreted. The wiggles seen on the curves are z-oscillations of the reaccreting material around the disk plane. If the ram pressure pulse is high enough (right), it kicks abruptly the disk, which accelerates the outer ISM directly to the v_{esc} and shifts only the inner ISM out of the disk plane. Consequently, ∼ 52% of the ISM moves out of the $|z| < 1$ kpc layer, but more than a half of it, i.e. ∼ 30% of the original amount of the ISM,

Fig. 12. Stripping of the LM–type galaxy in central parts of clusters with fixed $R_{c,ICM} = 13.4$ kpc and varying $\rho_{0,ICM}$: 0.25, 0.5, 1, 2, and 4 x 4 10^{-3} cm^{-3} (top row, from dashed to dot-dot-dot-dashed) and with fixed $\rho_{0,ICM} = 4 \ 10^{-3}$ cm^{-3} and varying $R_{c,ICM}$: 0.25, 0.5, 1, 2, and 4 x 13.4 kpc (bottom row, from dashed to dot-dot-dot-dashed). Evolution of the ISM mass bound to the galaxy (left) or staying within $r < 16$ kpc and $|z| < 1$ kpc about the disk plane (right) is displayed. Reaccretion of the stripped ISM is observable.

remains gravitationally bound and is later reaccreted. It may be seen as a deep notch with the deepest part at T ~ 1.65 Gyr.

b) Following a column, i.e. for a fixed value of the central density, the stripping begins in wider clusters at earlier times, since the value of the ram pressure sufficient to affect the outer ISM shifts to larger distances from the cluster center. Thus, the minimum of the ISM mass in the evaluation zone $|z| < 1$ kpc broadens. Broad clusters, with $R_{c,ICM} = 53.6$ kpc, are not only much more effective in removing the ISM particles outside the $|z| < 1$ kpc layer, but the more extended ram pressure pulse is also able to accelerate more ISM and remove it from the parent galaxy.

Table 3 quantifies the stripping results of the set of twenty-five simulations and adds values of parameters characterizing individual runs. One sees that in a small (low and narrow) cluster, poor in ICM, where $\rho_{0,ICM} = 1 \ 10^{-3}$ cm^{-3} and $R_{c,ICM} = 3.4$ kpc, the LM–type galaxy is stripped of less than 1% of its ISM only. It happens between the orbital time 1.53 and 1.64 Gyr. On the other hand, a large (high and wide) cluster with a lot of ICM, where $\rho_{0,ICM} = 1.6 \ 10^{-2}$ cm^{-3} and $R_{c,ICM} = 53.6$ kpc, the stripping of 85% of the ISM is achieved between orbital times 1.37 and 1.56 Gyr.

Fig. 12 summarizes the results of the set of simulations. The general trends that galaxies crossing wider and higher ICM density peaks lose a growing amount of the ISM, and that the reaccretion weakens, are clearly visible. In clusters with a constant width, the stripping starts within a short time range, while it occurs earlier in wide clusters, where
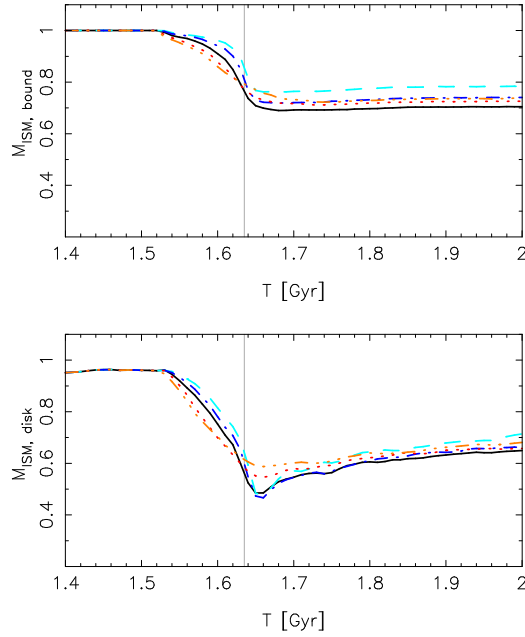
galaxies fall faster towards the cluster center and the ICM has a larger extent.

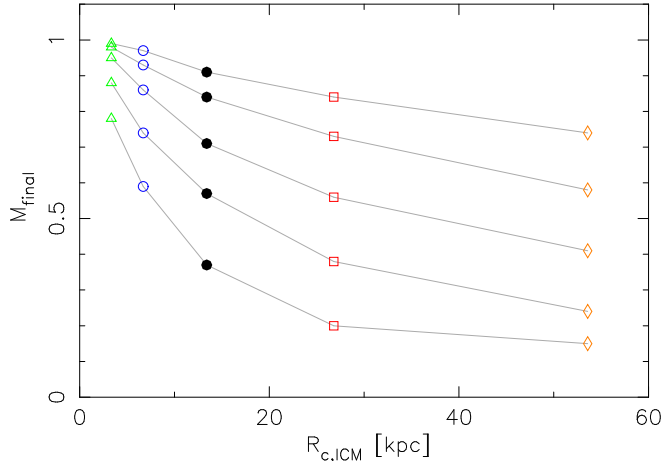### 6.2.2. Comparison with the criteron of Gunn & Gott

Focusing in Table 3 on values of the column density of the encountered ICM, we note that the passages through clusters with a similar amount of the encountered ICM show a similar amount of the stripped ISM. Fig. 13 compares the process of stripping in five clusters with $\Sigma_{ICM} \sim (5-6)$ M$_\odot$/pc^2 which are in Table 3 marked in boldface. In their case, $M_{strip} = 22\%, 26\%, 29\%, 27\%$, and 26%. However, the stripping history differs: in a narrow cluster with a high ICM density peak, there is a lot of ISM shifted out of the $|z| < 1$ kpc zone, but which is reaccreted later. In a broad cluster with a rather shallow density peak, more ISM stays near the galaxy symmetry plane and one sees less of the reaccretion.

The two extreme cases substantially differ in the peak ram pressure, in the first case it is almost 16 $\times$ higher compared to the second case. Gunn & Gott (1972) criterion (Eqn. 1) would predict a completely different amount of stripping in these cases. However, as we shall argue later, the final stripping depends on column density of the encountered ICM, which is similar in the two cases. In Fig. 18 a comparison of the simulation results with Gunn & Gott (1972) predictions can be seen.

In Fig. 14 the dependence of the remaining gas mass fraction $M_{final} = 1 - M_{strip}$ on the extent of the ICM distribution in the cluster is plotted. For increasing $R_{c,ICM}$, the degree of stripping becomes less and less dependent

Gal. type	R_{strip} (kpc)	M_{strip} (%)	M_{min} (%)	M_{accr} (%)
LM	6.3	29	49	22
Lm	3.9	59	27	14
EM	2.9	73	18	9
Em	0.2	96	4	0

Table 4. Stripping results for different galaxy types in the standard cluster.

Fig. 13. Stripping of the LM–type galaxy in different clusters but with a similar amount of the encountered ICM, $\Sigma_{ICM} \sim (5-6)$ M$_\odot$/pc^2. Curves correspond to $(R_{c,ICM}, \rho_{0,ICM}) = (3.4, 16)$ – dashed, $(6.7, 8)$ – dot-dashed, $(13.4, 4)$ – solid, $(26.8, 2)$ – dotted, and $(53.6, 1)$ – dot-dot-dashed in units (kpc, 10^{-3} cm^{-3}). The ISM mass bound to the galaxy (top) or staying within $r < 16$ kpc and $|z| < 1$ kpc layer about the disk plane (bottom) are displayed. Vertical line indicates the instant of the galaxy's passage through the center of the standard cluster.

Fig. 14. Final ISM mass fraction M_{final} as a function of $R_{c,ICM}$ for the LM–type galaxy. The lines correspond to different values of the $\rho_{0,ICM}$: 1, 2, 4, 8, and 16 cm^{-3} (from top down).

on the size of the ICM distribution (characterized by the $R_{c,ICM}$ itself) and approaches a constant, which depends on the value of $\rho_{0,ICM}$. This depends on whether or not the ISM is accelerated during the ram pressure pulse to the escape velocity. The critical size of the active region ΔR_C is $\Delta R_C = v_{esc} \, v \, \Sigma_{ISM}/P_{ram}^{eff}$, where P_{ram}^{eff} is an effective value of the ram pressure. Here we take $P_{ram}^{eff} = P_{ram}^{max}/2$. With $\Sigma_{ISM} = 10^{21}$ cm^{-2}, $v_{esc} = 400$ km/s, $P_{ram}^{max} = 6000$ cm^{-3}km^2 s^{-2} and $v = 1300$ km/s we get $\Delta R_c \approx 60$ kpc.

This nicely corresponds to $R_{c,ISM} = \Delta R_c/2 = 30$ kpc (see Fig. 14), where M_{final} loses its dependence on $R_{c,ISM}$ and converges to Gunn & Gott (1972) prediction given with (Eqn. 1). Thus, our results give much less stripping compared to Gunn & Gott (1972) in clusters with a narrow ICM peak, while converge to its predictions in extended ICM clusters.
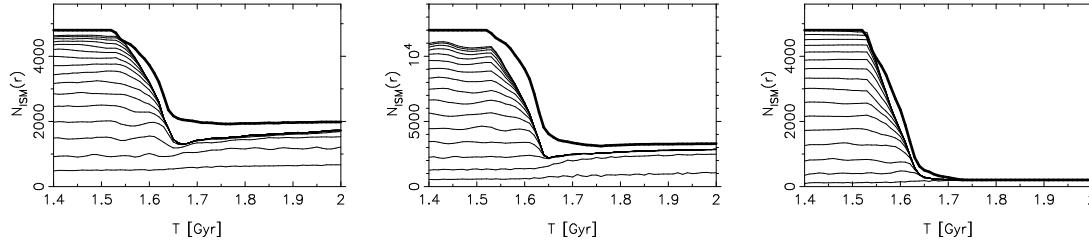
6.3. Various galaxy types

A comparison of the models Lm, EM, and Em in the standard cluster is shown in Fig. 15. The LM–type galaxy has a stripping radius of about 6 kpc, and loses about 29% of its original ISM. For Lm, and EM–type galaxies the stripping radii move closer to the galaxy center, to about 3.9 kpc, and 2.9 kpc, respectively. The Em–type galaxy is stripped almost completely. As summarized in Table 4, the LM, Lm, EM, and Em galaxy types lose during the face-on motion through the cluster with standard ICM distribution about 29%, 59%, 69%, and 96% of its original ISM.
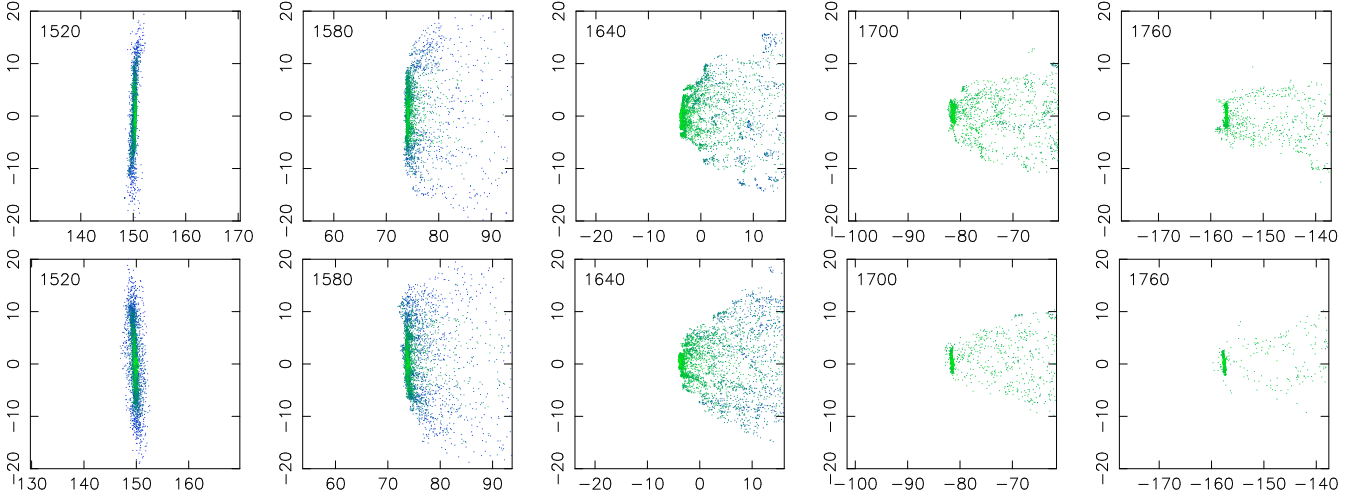
We may ask why is the amount of the stripping smaller in the case of the Lm–type compared to the EM–type, when except the innermost radii, the maximum restoring force is larger for the EM galaxy (see Fig. 2, left panel). However, in the range $(1-4)$ kpc, where the stripping radii of the two cases reside, the maxima of the restoring forces are almost equal. Further, the surface density of the ISM is lower, and the escape velocity is higher in the EM–type compared to the Lm–type. But, as we shall see later, the combination of a lower escape velocity and a higher Σ_{ISM} in the Lm–type does not explain less stripping compared to the EM–type.

As shows Fig. 2, right panel, the maxima of the restoring force over z-direction occur substantially closer to the disk plane in the case of the Lm galaxy, especially at low galactic radii. Thus, the rise of the restoring force behind the disk is much steeper in the Lm galaxy than in the EM model. In both cases, the galaxies move through the narrow standard cluster. Consequently, the ISM of the Lm–type galaxy is by the short ICM wind just shifted only "slowly" out of the disk. On the contrary, the ISM in the EM–type galaxy is by the same ram pressure more easily shifted to higher z's, and is thus during a longer time accelerated towards the v_{esc}.

The difference in the amount of delivered ICM momentum has also hydrodynamical reasons: the higher density of the ISM leads to creation of a larger and stronger

Fig. 15. Evolution of the stripping of the Lm, EM, and Em galaxy types (from left to right) during their crossing of the standard cluster.

Fig. 16. Edge-on snapshots of the stripping of the Lm (top) and EM (bottom) galaxies. The ISM disk of the EM galaxy type is clearly thicker in comparison with the Lm–type before they enter the ICM distribution.

bow shock, better protecting the ISM against the incoming ICM, that is more effectively deflected to the sides, causing the ISM in Lm–type gets less ICM momenta compared to EM galaxy.

Fig. 16 displays five snapshots of the Lm and EM galaxies during their passage through the central parts of the standard cluster. The ISM disk of the EM–type galaxy is due to its higher bulge-to-disk mass ratio much thicker than that of the Lm–type. This brings another possible explanation of the more effective stripping of the EM galaxy: its thicker disk is more vulnerable to the ram pressure.
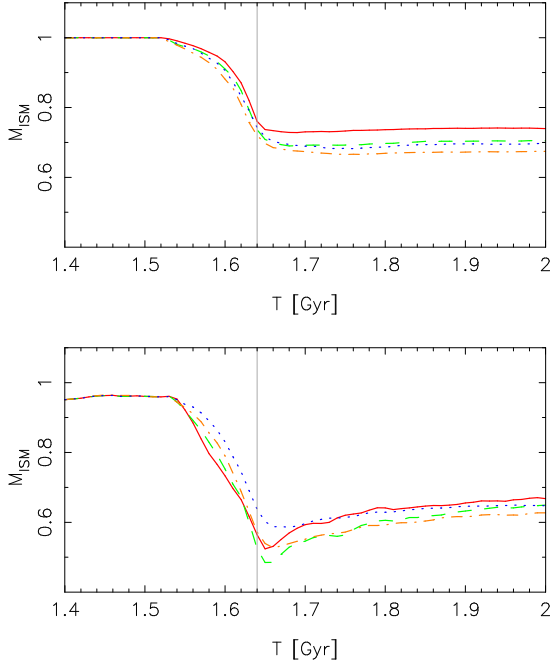
7. Simulation tests

To test the influence of the number of ICM particles, we vary N_{ICM}, by a multiplicative factor α. Then, since the SPH number of neighbors is fixed, the smoothing lengths evolve as $h' = h\,\alpha^{-1/3}$. We have performed a set of test runs with the LM–type galaxy crossing the standard cluster with a number of ICM particles varying as 480 000, 120 000, 24 000, and 12 000. Fig. 17 displays the results – the time evolution of the ISM mass bound to the galaxy (top), and the ISM mass located within the $r < 16$ kpc, $|z| < 1$ kpc zone (bottom). Although the number of ICM particles differs by a factor 40 in the extreme cases, which corresponds to about 3.4-fold difference in the SPH par-

ticle sizes, only a small difference in the final stripping results is observed in Fig. 17.

In the case of $N_{ICM} = 12\,000$, the ICM particles are so large, that every one of them can cover a substantial part of the disk. Then instead of a detailed hydrodynamical interaction, the ISM particles in the disk feel only a global ram pressure of a few large ICM particles. As the number of ICM particles in the simulation increases, the hydrodynamical interactions are treated in a better way, since the mutual sizes of ICM and ISM particles approach. However, Fig. 17 demonstrates that the stripping results are almost independent of the size of the ICM particles, which means that the detailed hydro-effects (like turbulence etc.) play only a minor role in the process of stripping. The dominant process which governs the sweeping is the ram pressure.

Fig. 17 further depict that due to smoothing of the ICM peak by increasing sizes of the particles, shifting of the ISM out of the $|z| < 1$ kpc evaluation zone is steeper, and the minima of the ISM mass within the evaluation zone are deeper for higher N_{ICM}.

Apart from changing sizes of the ICM particles, the growing value of the N_{ICM} causes different mass ratios of individual ICM vs. ISM particles: 10.3, 5.2, 1, and 0.26.

Fig. 18. The final mass fraction M_{final} of the gas which remains in the disk after the stripping events as a function of the maximum value of the ram pressure p_{ram}. The symbols denote the results of the SPH calculations for the five groups of clusters with various values of the $R_{\mathrm{c,ICM}}$: 3.4 kpc (triangles), 6.7 kpc (circles), 13.4 kpc (filled circles), 26.8 kpc (squares), and 53.6 kpc (diamonds), while the gray curves are the corresponding predictions obtained by integration of Eqn. 5. The thick solid line refers to the criterion of Gunn & Gott (1972), Eqn. 1.

Fig. 17. Simulation results of the LM–type galaxy crossing the standard cluster with varying number of ISM particles: 480 000 (full), 120 000 (dashed), 24 000 (dot-dashed), and 12 000 (dotted). Total mass of the bound ISM (top), and of the ISM located within $r < 16$ kpc, $|z| < 1$ kpc zone about the disk plane (bottom), are displayed as functions of the orbital time.

8. Analytical model

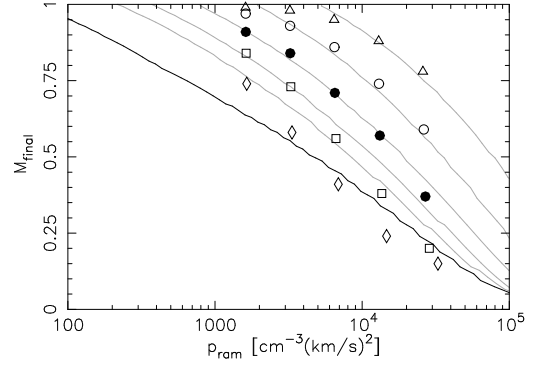### 8.1. The equation of motion of an ISM element

After presenting our numerical results in the previous section, we consider the interaction of the galactic ISM with the ICM from an analytic point of view. We describe the trajectory of an individual ISM element originally sitting in the disk plane, as it moves under the influence of the cluster gravity forces, the restoring force of the galaxy, and the ICM pressure force.

As shown in the simulations, a bow shock forms when the incoming ICM arrives to the galaxy's disk. Consequently, the ICM decelerates at the shock, transferring part of its momentum to the galaxy, and flows along the shock envelope around the disk. The disk itself feels the pressure of the bow shock and thus the ISM is pushed out of the disk plane, against the galaxy restoring force.

Disregarding the above hydrodynamical effects, and considering the face-on case, the equation of motion (EOM) for the movement of an ISM element in z-direction, i.e. vertical to the galactic plane, is

$$\frac{d\left(v_{out}\Sigma_{\mathrm{ISM}}\right)}{dt} = \rho_{\mathrm{ICM}}(v - v_{out})^2 - \frac{\partial\Phi}{\partial z}\Sigma_{\mathrm{ISM}}, \qquad (5)$$

where v is the galaxy's orbital velocity. The rightmost term is the gravitational restoring force at the current z-position of the ISM element, whose current velocity is v_{out} with respect to the galaxy's rest frame. The ISM element feels a reduced ram pressure because of the relative velocity of the galaxy and the ICM, v, is reduced by v_{out}.
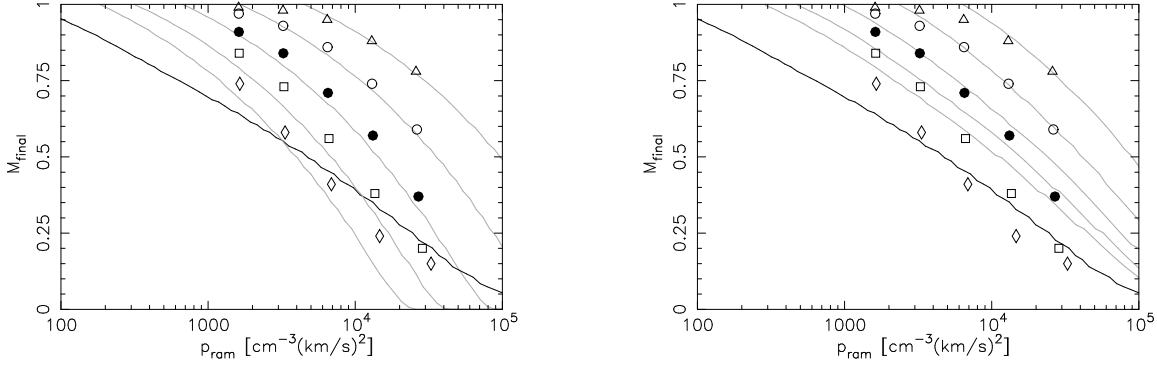
When v_{out} exceeds the local value of the escape velocity $v_{esc}(r, z)$, the element is stripped.

The solution of this equation together with $dz/dt = v_{out}$ gives the speed and the trajectory of the ISM element in the gravitational field of the galaxy and under the influence of the changing ram pressure. From Eqn. 5 one notes that apart from the actual value of the ram pressure reduced by the local restoring force, the history of the encountered ICM also matters. In the disk of a galaxy one applies this EOM to the ISM at each galactocentric radius and by numerical integration one can follow the fate of each annulus of the disk until it is stripped. The stripping radius r_{strip} is a radius above which $v_{out}(r)$ exceeds the value of the escape velocity in the galactic plane. The final mass then is determined as the mass of the ISM mass enclosed within the stripping radius, according to the density profile in the disk (Eqn. 3).

Fig. 18 compares these predictions of Eqn. 5 with the results of the SPH simulations, depicting M_{final} as a function of the peak value p_{ram} of the ram pressure. One notes that the curves from the simple EOM model match rather well the results obtained by the SPH simulations, in particularly for narrow clusters with $R_{\mathrm{c,ICM}} = 3.4$, 6.7, and 13.4 kpc. For large clusters, the simple model underestimates the stripping severely. This may be because in Eqn. 5 we neglect the deformation of the stripped ISM disk which would affect the restoring force, or none of the hydrodynamical effects is taken into account. Nonetheless, this very simple approach reproduces the dependence on both the extend and the density of the cluster quite well.

Fig. 18 also shows that the criterion of Gunn & Gott (1972) constitutes the limit for maximum possible stripping. The final mass fractions predicted from the simple approach converge towards the estimates based on Eqn. 1 at high values of $R_{\mathrm{c,ICM}}$ and $\rho_{0,\mathrm{ICM}}$, but they always remain larger. This is because Gunn & Gott (1972) assume

Fig. 19. Numerical results versus analytic predictions of Eqns. 8 (left) and 9 (right) of final remaining gas mass fraction M_{final} after the stripping events as functions of the maximum value of the ram pressure p_{ram}. The symbols for individual simulations are the same as in Fig. 18. The thick solid line corresponds to Gunn & Gott (1972), Eqn. 1.

a constant operation of the peak value of the ram pressure and compare it with the maximum restoring force. Therefore, at all radii of the disk, where the (peak) ram pressure exceeds the maximum restoring force, all the ISM elements can be accelerated to the escape velocities. However, in the integration of the EOM, an ISM element may cross the z-distance of the maximum restoring force, but the peak of the ram pressure may be over before the element reaches escape velocity.

8.2. The impulse approximation

Since our principal intention is not to follow the exact trajectory of the stripped elements but only to identify them and thus obtain the stripping radius (or the final mass), let us introduce an approximative solution of the EOM.

If we consider only those regions where the gas is clearly removed from the galaxy disk, we can obtain a first order solution by considering the balance of the momentum. Neglecting the restoring force in these outer regions, the momentum per unit surface area attained by the stripped gas, of surface density Σ_{ISM}, and velocity v_{after} is

$$P_{after} = v_{after}\Sigma_{\mathrm{ISM}} = \int \rho_{\mathrm{ICM}}v^2 dt, \qquad (6)$$

This quantity P_{after} can be considered as the integrated history of the ram pressure:

$$P_{after} = \Sigma_{\mathrm{ICM}}\frac{\int \rho_{\mathrm{ICM}}v^2 dt}{\int \rho_{\mathrm{ICM}}v dt} = \Sigma_{\mathrm{ICM}}\langle v\rangle_{\rho_{\mathrm{ICM}}}, \qquad (7)$$

where $\Sigma_{\mathrm{ICM}} = \int \rho_{\mathrm{ICM}}v dt$ is the column density of the encountered ICM, and $\langle v\rangle_{\rho_{\mathrm{ICM}}}$ is the averaged velocity v along the galaxy's orbit weighted with the local volume density ρ_{ICM}. Then Eqn. 6 becomes

$$v_{after} = \langle v\rangle_{\rho_{\mathrm{ICM}}}\frac{\Sigma_{\mathrm{ICM}}}{\Sigma_{\mathrm{ISM}}}. \qquad (8)$$

Of course, the restoring force f_{rest} can only be neglected in the stripped outer parts of the galaxy. A better

approximation of the EOM is to consider the momentum transferred from the inflowing ICM to the ISM element after the element passed the position z with maximum value of the restoring force. Thus, one regards the acceleration of the ISM only when the ram pressure exceeds this maximum. Then, at a given radius,

$$v_{after} = \frac{\int \left(\rho_{\mathrm{ICM}}v^2 - \frac{\partial \Phi}{\partial z}|_{\max}\Sigma_{\mathrm{ISM}}\right)dt}{\Sigma_{\mathrm{ISM}}}, \qquad (9)$$

where the integration is taken over a time interval (t_1, t_2) when $p_{ram} > f_{rest,max}$, i.e. as long as the Gunn & Gott (1972) criterion (Eqn. 1) is fulfilled. Since the actual value of the restoring force at the position (r, z) is less compared to its maximum value, this obviously overestimates the binding of an element to the galaxy plane.

Fig. 19 shows a comparison of the results of the SPH simulations and from the approximative solutions by Eqns. 8 and 9 which are expected to bracket the actual equation. As before, the stripping radius r_{strip} is the radius above which $v_{after}(r)$ exceeds the value of the escape velocity in the $z = 0$ plane. Then the final mass is determined as the mass of the ISM enclosed within the stripping radius, according to the disk's density profile (Eqn. 3). One notes that the curves from Eqn. 8, which neglects the restoring force, indeed overestimate the stripping, while curves based on Eqn. 9, which consider only the momentum gained as long as the ram pressure exceeds the maximum restoring force, underestimate the stripping. In any case, the departures from SPH results are larger than with the predictions of the EOM (Eqn. 5), displayed in Fig. 18.

Of course, comparing the full numerical treatment with the predictions of the analytical approach may have several caveats. The most important is that all the hydrodynamical processes, such as the effect of the bow-shock and size of the galaxy shadow, are disregarded in the solution which describes the dynamics of a single ISM element. Furthermore, in the analytic calculations, the density profile of the ISM is assumed to be constant, whereas in the full simulations processes of relaxation and formation of spiral arms, as well as the progressive stripping, can change the surface density profile of the gas disk. Such

changes consequently affect the restoring force, and the escape velocity profiles.

Nonetheless, it is interesting that the simple conservation of momentum (Eqn. 8), which on one side neglects the actual effect of the restoring force and the element's shifting out of the disk, and on the other side overestimating the escape velocity and changes of the ISM disk due to stripping, can give a good order of magnitude estimate of the stripping, when the variation of the ICM density along the galaxy's path is to be taken into account. The Gunn & Gott (1972) formula, computed only from the maximum ICM density, overestimates the stripping, and does not permit to predict the effect of the finite size of the cluster, i.e. the finite time of interaction. However, in cases with large values of $R_{c,\mathrm{ICM}}$ and $\rho_{0,\mathrm{ICM}}$ the SPH simulations show an even larger stripping than the Gunn & Gott (1972) estimate. This may be a consequence of uneven gas distribution in the galaxy disk where spiral arm inhomogeneities contribute to the ISM removal as also shown by Quilis et al. (2000).

9. A comparison to other simulations

9.1. Abadi et al. (1999)

Performing 3D SPH/N-body simulations, Abadi et al. (1999) study the stripping of spiral galaxies by operation of a constant flow of ICM particles in a simulation box of size 60 kpc × 60 kpc × 10 kpc homogeneously filled up with the ICM particles flowing with periodic boundary conditions. Their model is a spiral galaxy receiving the wind of 1000 km s^{-1}, 2000 km s^{-1}, or 3000 km s^{-1} of density: $\rho_c = 3.37\ 10^{-3}$ cm^{-3}, and $\rho_v = 0.1\rho_c$, corresponding to central densities of the Coma and Virgo cluster, respectively. The ram pressure then ranges from about 300 to 30 000 cm^{-3}km^{2}s^{-2}. For the Coma-like ICM density, they estimate the stripping radius of a spiral galaxy to 4 kpc, i.e. to about 80 % loss of the galaxy's diffuse gas mass.

9.2. Quilis et al. (2000)

In their simulations employing a high resolution 3D Eulerian code with a fixed grid based on high-resolution shock-capturing method, Quillis et al (2000) follow the interaction between the hot ICM and the cold ISM. The stellar and DM components are evolved using a particle-mesh code. They model a luminous spiral galaxy similar to the Milky Way or Andromeda. The ICM is modelled as a uniform medium with temperature $T_{\mathrm{ICM}} = 10^8$ K and a constant densities $\rho_c = 2.6\ 10^{-3}$ cm^{-3}, and $\rho_v = 0.1\rho_c$. The galaxy moves through the ICM wind at velocities of 1000 km s^{-1}, or 2000 km s^{-1}. For the Coma-like ICM density and velocity, they estimate the stripping radius to ~ 3 kpc.

9.3. Vollmer et al. (2001)

Investigating the role of the ram pressure stripping in the Virgo Cluster, Vollmer et al. (2001) employ a method of sticky particles for modelling the warm neutral clouds of the ISM. The effect of the ram pressure is included only analytically as an additional acceleration on the clouds located at the windward side of the gas distribution. Contrary to other simulations discussed in this section, they introduce temporal ram pressure profiles in their simulations instead of a constant ICM wind. They use the model of a spiral galaxy in a wind creating the ram pressure reaching maximum values ranging from 1 000 to 10 000 cm^{-3}km^{2}s^{-2}. Galaxies on slightly elliptical orbits not reaching the very center of the cluster are considered. It means that their maximum ram pressure is lower as corresponding to the central value of ICM density and maximum infall velocity, and that the effective size of the interacting region is larger than it would be on completely radial orbit with the same maximum ICM density encountered and width $R_{c,ICM}$ equal to its original value. They show that the ram pressure can lead to a temporary increase of the central gas surface density, and that in some cases a strong reaccretion of the atomic gas occurs after the stripping event. They find that the scenario of ram pressure stripping being responsible for the observed H I deficiency is consistent with all HI 21 cm observations in the Virgo Cluster.

9.4. Schulz & Struck (2001)

A model a dwarf galaxy in 3D HYDRA (SPH-AP^{3}M) simulations of Schulz & Struck (2001) is placed in a cubical grid with 100 kpc edge. The galaxy is surrounded with 80 000 uniformly distributed ICM particles. The temperature of the ICM is $T_{\mathrm{ICM}} = 4.6\ 10^5$ K, and the density of the wind is $\sim 7.3\ 10^{-5}$ cm^{-3}. In their face-on models, the galaxy moves with a velocity of 1000 km s^{-1}, or 2000 km s^{-1}. Then, the stripping radii measured from their Figs. 2 and 14 are ~ 7.2 kpc and ~ 5.2 kpc.
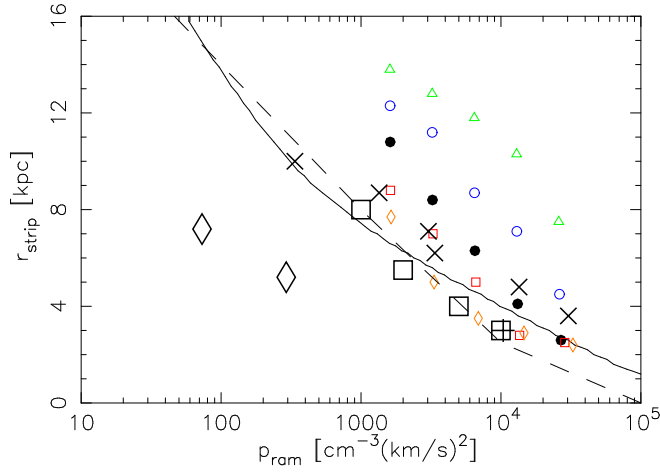
9.5. Roediger & Hensler (2005)

With a spiral galaxy models and a large range of ICM conditions, Roediger & Hensler (2005) perform a parameter study of the ram pressure stripping using a 2D Eulerian simulations. Except the gaseous disk, all components are treated analytically, providing only the gravitational potential. The ICM densities range from 10^{-5} to 10^{-3} cm^{-3}, and the resulting ram pressure covers a range from 10 to 10 000 cm^{-3}km^{2}s^{-2}.

9.6. Summary

The different simulations are listed in Tab. 5 and a comparison is shown in Fig. 20. All the models shown, except Schulz and Struck (2001), use comparable spiral

Fig. 20. r_{strip} versus the peak ram pressure p_{ram}^{max}: a comparison with simulations by Abadi et al. (1999) – large X, Quilis et al. (2000) – large plus, Vollmer et al. (2001) – large squares, Schulz & Struck (2001) – large diamonds, models of Roediger & Hensler (2005) – dashed line. Our simulations: $R_{c,ICM}$ = 3.4 kpc – triangles; 6.7 kpc – circles; 13.4 kpc – filled circles; 26.8 kpc – squares; 53.6 kpc – diamonds. Solid line shows the prediction using Gunn & Gott (1972) (Eqn. 1).

Author	Method	ICM flow	galaxy
Abadi	SPH	constant	spiral
Quilis	3D finite diff.	constant	spiral
Vollmer	sticky particle	changing	spiral
Schulz	SHP	constant	dwarf
Roediger	2D finite diff.	constant	spiral
Jáchym	SPH	changing	spiral

Table 5. The list of simulations.

10. Discussion and conclusions

The simulations performed in the present work allow us to better estimate the consequences of ram pressure stripping in clusters. If a galaxy like the Milky Way (our type LM) passes through the center of a cluster similar to Virgo (our standard cluster) in a purely radial trajectory and in face-on orientation, it loses about 29% of its interstellar gas. This constitutes a rather important amount of gas loss, but it is a maximum value, because the galaxy passes exactly through the central peak of the ICM.

According to additional simulations of ours, to be published elsewhere, and to Roediger & Brüggen (2006) the efficiency of stripping only marginally depends on the orientation of the galaxy. Therefore, we shall disregard this aspect in this discussion.

With this level of stripping, we may estimate the fraction of gas supplied to the ICM by stripping: The amount of gas lost by a LM-type galaxy is about $2 \cdot 10^9$ M$_\odot$. A much less massive Lm-type galaxy is more severely stripped, thus providing roughly the same amount of gas. EM and Em-types are subject to an even more effective stripping, but their gas disks are less massive. Our estimate is that the average contribution per spiral galaxy, late or early type, with different orientations in a radial orbit, is 1 - 2 10^9 M$_\odot$. This means that the total amount of hot gas in the central region of our standard cluster ($6 \cdot 10^{10}$ M$_\odot$) can be provided by 30 - 60 stripping acts. The amount of stripping from past to present is influenced with the decreasing gas content of galaxies, which is an obvious consequence of gas consumption by star fomation: gas-rich galaxies in the past can provide more gas to intergalactic space. On the opposite, the growing ICM concentration in the center of the cluster leads to higher stripping efficiency now.

Note than only the contribution from galaxies on radial orbits is substantial. Galaxies on circular or elliptical orbits do not penetrate the dense parts of the ICM and thus are safe from being stripped. Depending on the fraction of galaxies in radial orbits in the cluster, which unfortunately is not well known, the stripping could supply a significant amount of gas to the ICM. This may explain the high metallicity of the ICM gas.

Another consequence of our simulations is that we expect to find in any cluster a significant amount of relatively cold gas, as debris left over from recent stripping events. This gas is not yet mixed with the ICM, but forms large diffuse clouds as tails behind the galaxy keeping a fraction of its velocity. The mixing time should be compa-

galaxy models. Abadi et al. (1999), Quilis et al. (2000) and Roediger and Hensler (2005) show high stripping efficiency close to the Gunn & Gott (1972) prediction, which is due to a constant ICM density adopted. There is no difference in the stripping radius and M_{final} from 2D and 3D hydrodynamical simulations and SPH. It seems that the global stripping effect on the galaxy does not depend on the details of the hydrodynamical approach.

The results of Schulz and Struck (2001) show the same stripping efficiency at lower ram pressures (see Fig. 20), which is, in accordance to Gunn & Gott(1972), due to lower disk restoring force in the case of dwarf galaxies.

Our models with small values of $R_{c,ICM}$ show less stripping. This is mainly due to the effect of changing strength and finite duration of the ram pressure peak. For large values of $R_{c,ICM}$ in large clusters with long interaction times our models approach the Gunn & Gott (1972) prediction and results of other models. It demonstrates that our SPH approach gives similar results to SPH simulations of others and to 2D and 3D Eulerian codes.

Simulations by Vollmer et al. (2001) use the changing ram pressure force acting on sticky particles showing results close to Gunn and Gott (1972) prediction. However, with the similar dependence of the ram pressure on time, we get less stripping. Simulations with sticky particles probably overestimate the stripping efficiency, since this kind of simulations disregards such hydrodynamical effects as formation of the bow shock in the ICM in front of the galaxy. It actually shields the galaxy reducing the efficiency of stripping.

rable to the free-fall time, e.g. ~ 1 Gyr. The density of gas in tails may be more than 10 times larger than the local hot ICM density, hence a tail could cause strong stripping for any galaxy which happens to cross it at a very different velocity. This can then provide a nice explanation to the puzzling strong stripping recently observed in many regions where the hot ICM gas is not sufficient to strip. For instance NGC 4522 is apparently stripped at a large distance from the cluster center (Crowl & Kenney 2006), where the ICM density is not sufficient. A nice example of a cold HI tail almost 100 kpc long provides the galaxy CGCG 97-073 in the Coma cluster. This and similar tails may be the cause of ram pressure for other galaxies arriving at high speed.

Also ram-pressure stripping appears in small groups, where the X-ray gas is not detected (Rasmussen et al 2006). As we have shown in the paper, the crucial effect of the ram pressure stripping is the pressure itself, the hydrodynamical effects play only a minor role. Therefore, not only the hot ICM is able to strip the galactic ISM, but debris from tidal interactions or previous stripping as well.
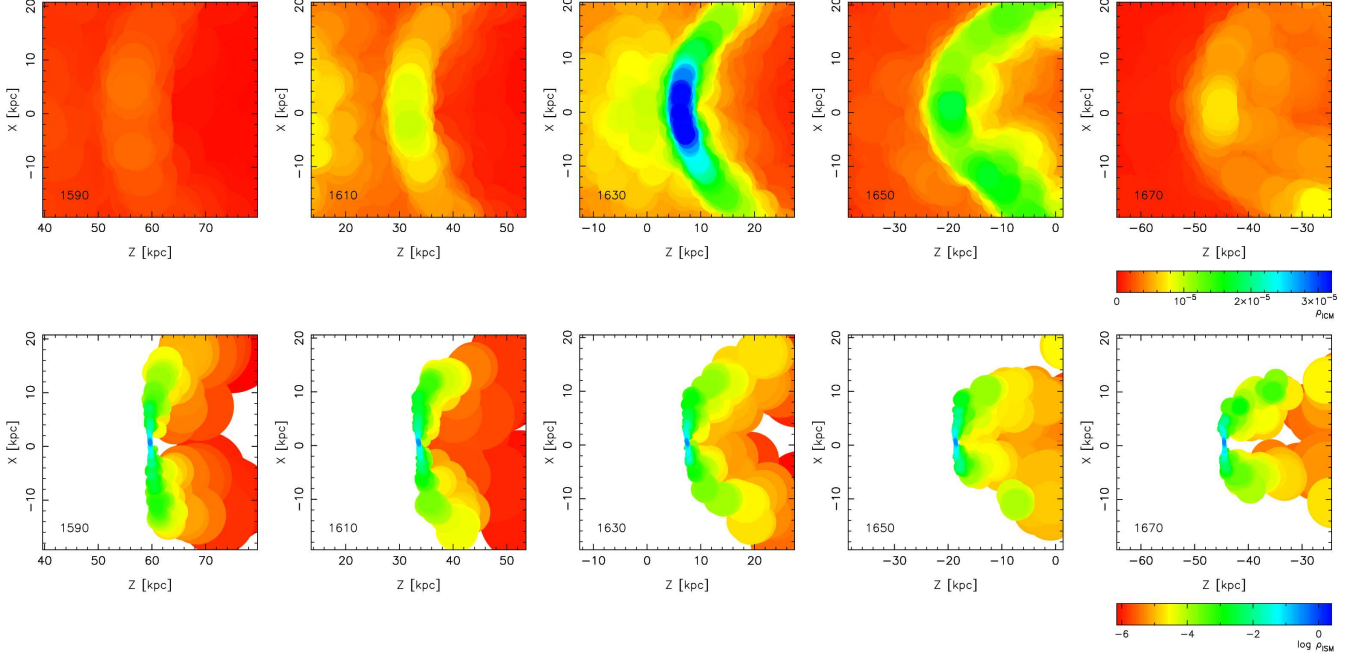
The main conclusion is that the stripping efficiency depends significantly on the duration of the ram pressure pulse, which in many cases means that Gunn & Gott (1972) prediction overestimates the amount of stripping. This is nicely shown by Boselli & Gavazzi (2006, their Fig. 18), where they compare the restoring force in spiral galaxies in Coma, A1367 and Virgo clusters to the maximum ram pressure. It turns that many galaxies with normal HI content should have been stripped if the ram pressure had acted for a sufficiently long time. Much more modest stripping is observed showing that Gunn & Gott (1972) prediction is an overestimation.
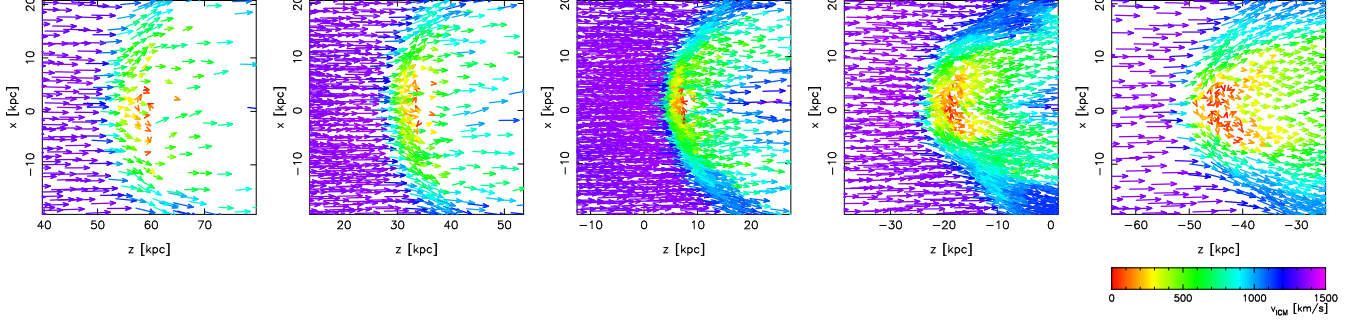
References

Abadi, M. G., Moore, B., & Bower, R. G. 1999, MNRAS 308, 947

Acreman, D.M., Stevens, I.R., Ponman, T.J., Sakelliou I. 2003, MNRAS 341, 1333

Arnaboldi, M., Freeman, K. C., Okamura, S., et al. 2003, AJ 125, 514

Barnes, J., Hut, P. 1986, Nature 324, 446

Boselli, A., Gavazzi, G. 2006, PASP 118, 517

Böhringer, H. 2004, IAU Symp. 217, 92

Böhringer, H., Briel, U., G. Schwarz, R. A., et al. 1994, Nature 368, 828

Cavaliere, A., & Fusco-Femiano, R. 1976, A&A 49, 137

Crowl H.H., Kenney J.D.P. 2006, ApJ L in press (astro-ph/0608229)

Domainko, W., Gitti, M., Schindler, S., & Kapferer, W. 2004, A&A 425, L21

Domainko, W., Mair, M., Kapferer, W., van Kampen, E., Kronberger, T., Schindler, S., Kimeswenger, S., Ruffert, M., & Mangete, O. M. 2005, astro-ph/0507605

Fabian, A. C. 1994, ARAA 32, 277

Finoguenov, A., Peitsch, W., Aschenbach, B., & Miniati, F. 2004, A&A 415, 415

Gingold, R. A., Monaghan, J. J. 1977, MNRAS, 181, 375

Gunn, J. E., & Gott III, R. J. 1972, ApJ 176, 1

Kundić, T., Spergel, D. N., & Hernquist, L. 1993, AAS 183, 8708

Lucy, L. B. 1977, AJ, 82, 1013

Mihos, J. Ch. 2004, IAU Symp. 217, 390

Moore, B., Katz, N., Lake, G., Dressler, A., & Oemler, A. Jr. 1995, Nature 379, 613

Murante, G., Arnaboldi, M., Gerhard, O. et al. 2004, ApJ 607, L83

Oosterloo, T., & van Gorkom, J. 2005, A&A 437, L19

Quilis, V., Moore, B., Bower, R. 2000, Science, 288, 1617

Rasmussen J., Ponman T.J., Mulchaey J.S. 2006, MNRAS 370, 453

Roediger, E., Brüggen, M., and Hoeft, M. 2006, MNRAS, 371, 609

Roediger E., Hensler G. 2005, A&A, 433, 875

Roediger, E., Brüggen, M. 2006, MNRAS, 369, 567

Schindler, S., Binggeli, B., Böhringer, H. 1999, A&A, 343, 420

Schindler, S., Kamferer, W., Domainko, W., Mair, M., van Kampen, E., Kronberger, T., Kimeswenger, S., Ruffert, M., Mangete, O, and Breitschwerdt, D. 2005, A&A 435, 25

Schulz, S., Struck, C. 2001, MNRAS, 338, 185

Springel V., Yoshida N., White S. 2001, New Astronomy, 6, 79

Vollmer, B., Soida, M., Otmianowska-Mazur, K., Kenney, J.D.P., van Gorkom, J. H., & Beck, R. 2006, astro-ph/0603854

Vollmer, B., Cayatte, V., Balkowski, C., & Duschl, W. J. 2001, ApJ 561, 708

Appendix

Fig. 21. Density of the ICM in surroundings of the LM–type galaxy (top) and of the ISM (bottom). $N_{\mathrm{ICM}} = 480\,000$. Particles are displayed as filled circles with radii equal to their SPH smoothing sizes. The ISM density scale is logarithmic. The time in Myr is given in the left lower corner of frames.

Fig. 22. The flow of ICM particles around the LM–type galaxy in the case of $N_{\mathrm{ICM}} = 480\,000$.